ARTICLE IN PRESS

Nano Energy (∎∎∎∎) ∎, ∎∎∎-∎∎∎

Available online at www.sciencedirect.com

ScienceDirect

journal homepage: www.elsevier.com/locate/nanoenergy

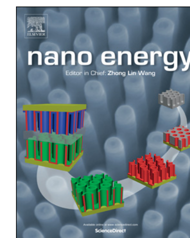

Fundamental theories of piezotronics and piezo-phototronics

Ying Liu[a], Yan Zhang[a,b], Qing Yang[a], Simiao Niu[a], Zhong Lin Wang[a,b,*]

[a]*School of Materials Science and Engineering, Georgia Institute of Technology, Atlanta, Georgia 30332-0245, United States*
[b]*Beijing Institute of Nanoenergy and Nanosystems, Chinese Academy of Sciences, Beijing, 100083, China*

Received 8 October 2014; received in revised form 14 November 2014; accepted 25 November 2014

KEYWORDS
Piezotronic effect;
Piezo-phototronic effect;
LED;
Solar cell

Abstract
Wurtzite structured mateirals such as ZnO, GaN, InN and CdS simultaneously exhibit piezoelectric, semiconducting and photoexcitation properties. The piezotronic effect is to use the inner crystal potential generated by piezoelectric polarization charges for controlling/tuning the charge carrier transport characteristics in these materials. The piezo-phototronic effect is about the use of piezoelectric charges to tube the generation, transport, separation and/or recombination of charge carriers at p-n junction. This article reviews the fundamental theories of piezotronics and piezo-phototronics, forming their basis for electromechancial devices, sensors and energy sciences. Starting from the basic equations for piezoelectricity, semiconductor and photoexcitation, analytical equations for describing the strain-tuned device current were derived. Through analytical calculations and numerical simulations, it was confirmed that the piezoelectric polarization charges can act in the form of inner-crystal charges in the depletion region, resulting in a change in Schottky barrier height, depletion region shift and/or formation of a charge channel, which can be used effectively to enhance the efficiency of LED, solar cell and photon detectors.
© 2014 Published by Elsevier Ltd.

Introduction

Piezoelectric materials have a wide range of applications in sensors, actuators and energy harvesting. In recent years, much attention has been focused on piezoelectric semiconductor materials in the Wurtzite family, such as ZnO, GaN, InN and CdS [1-7]. Due to the coupling of piezoelectric, semiconducting and photoexcitation properties, as shown in Fig. 1, the new fields of piezotronics and piezo-phototronics have been created. The piezotronic effect is to use the inner crystal potential generated by piezoelectric polarization charges for controlling/tuning the charge carrier transport characteristics and fabricating mechanical-electronic devices. Such devices

*Corresponding author at: School of Materials Science and Engineering, Georgia Institute of Technology, Atlanta, Georgia 30332-0245, United States
E-mail address: zlwang@gatech.edu (Z.L. Wang).

http://dx.doi.org/10.1016/j.nanoen.2014.11.051
2211-2855/© 2014 Published by Elsevier Ltd.

Please cite this article as: Y. Liu, et al., Fundamental theories of piezotronics and piezo-phototronics, Nano Energy (2014), http://dx.doi.org/10.1016/j.nanoen.2014.11.051

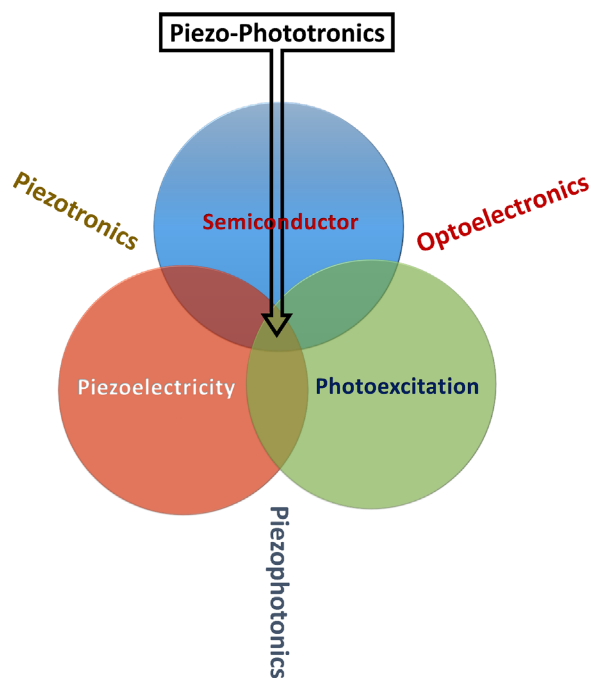

Fig. 1 Schematic diagram showing the three-way coupling among piezoelectricity, photo excitation and semiconductor properties.

can be the basis for active flexible electronics, which uses the mechanical actuation from the substrate for inducing new electronic/optoelectronic effects, with potential applications in micro-electromechanical systems, nanorobotics, human-computer interfacing and sensors [8]. The piezo-phototronic effect is about the use of piezoelectric polarization on the generation, transport, separation and/or recombination of charge carriers at p-n junction, in devices including photocells, photodetectors and LEDs, their performances and interaction with light are significantly changed by externally applied strain [9-11].

Since year 2008, abundant experimental studies have been reported to demonstrate the existence of the piezotronic and piezo-phototronic effects in ZnO, GaN and other Wurtzite structured material based devices [10-17]. In all these reports, several common phenomena are discovered: (i) strain can monotonically tune the device current; (ii) the change of device current switched polarity with the polarity of applied strain or direction of c-axis; (iii) photoresponse and photoemission can be dramatically enhanced by strain, and the enhancement of photoemission is much greater than the change of current; (iv) in devices with one p-n junction or Schottky junction on each end of the nanowires, asymmetric changes between positive biased current and negative biased current were recorded. To explain these observations, theoretical study will not only provide an in-depth understanding about these results, but also explore the core factors in this effect and build high performance devices.

Thus, from 2011, numerous theoretical analysis and numerical simulations have been performed to investigate the physics mechanisms behind the experimental results [18-20]. Starting from coupling the basic equations of piezoelectricity, semiconductor physics and photoexcitation, analytical equations of piezotronics and piezo-phototronics were derived. Specifically, the current-voltage characteristics of piezotronics/piezo-phototronics devices were expressed as functions of applied strain. The tuning effect of piezoelectric polarization was revealed in the relationship between device performance and mechanical deformation. Numerical simulations including Finite Element Method were then used to verify the analytical theory. Numerically simulated band structures confirmed the assumptions and conclusions from the analytical study. Taking into consideration the unideal factors, device current of both one-dimensional (1D) devices and two-dimensional (2D) devices were simulated and compared over strain range used in experiments, which intuitively demonstrated how the mechanism revealed could influence device performance, as well as extrapolate the basic theory into optimization methodology for future device designs. This review is intended to give a comprehensive coverage of the theoretical work done in piezotronics and piezo-phototronics in order to illustrate their fundamental understanding and intrinsic physics.

Theory of piezotronics [20]

Analytical solution for one-dimensional simplified p-n junction

The nature of piezotronics lies in the tuning effect of piezoelectric polarization on semiconductor behaviors. In most of the semiconductor devices, the formation of junctions at material interface is usually the essential part for realizing function of the device. Junction area is also where piezoelectric charges (piezo-charges) accumulate. The piezotronics effect could be evaluated by how strain tunes the current characteristics in devices such as a piezotronic sensor.

In piezotronics, the fundamental governing equations for both semiconductor and piezoelectric theories included electrostatic equations, current-density equations, continuity equations, [21] and the piezoelectric equations [22].

1) The Poisson equation is the basic equation for describing the electrostatic behavior of charges

$$\nabla^2 \psi_i = -\frac{\rho(\vec{r})}{\varepsilon_s} \tag{1}$$

where ψ_i is the electric potential distribution and $\rho(\vec{r})$ is the charge density distribution, and ε_s is the permittivity of the material.

2) The current-density equations that correlate the local fields, charge densities and local currents are

$$\begin{cases} \vec{J}_n = q\mu_n n\vec{\mathbf{E}} + qD_n\vec{\nabla}n \\ \vec{J}_p = q\mu_p p\vec{\mathbf{E}} - qD_p\vec{\nabla}p \\ \vec{J}_{\text{cond}} = \vec{J}_n + \vec{J}_p \end{cases} \tag{2}$$

where $\vec{J}_n$ and $\vec{J}_p$ are the electron and hole current densities, q is the absolute value of unit electronic charge, μ_n and μ_p are electron and hole mobilities, n and p are concentrations of free electrons and free holes, D_n and D_p are diffusion coefficients for electrons and holes, respectively, E is electric field, and $\vec{J}_{\text{cond}}$ is the total current density.

Please cite this article as: Y. Liu, et al., Fundamental theories of piezotronics and piezo-phototronics, Nano Energy (2014), http://dx.doi.org/10.1016/j.nanoen.2014.11.051

ARTICLE IN PRESS

3) The charge transport under the driving of a field is described by the continuity equations.

$$\begin{cases} \frac{\partial n}{\partial t} = G_n - U_n + \frac{1}{q}\vec{\nabla} \times \vec{J}_n \\ \frac{\partial p}{\partial t} = G_p - U_p - \frac{1}{q}\vec{\nabla} \times \vec{J}_p \end{cases} \quad (3)$$

where G_n and G_p are the electron and hole generation rates, U_n and U_p are the recombination rates, respectively.

4) The piezoelectric behavior of the material is described by a polarization vector P. For a small uniform mechanical strain ε_{jk}, [23] the polarization vector $\vec{\mathbf{P}}$ is given in terms of strain vector $\vec{\varepsilon}$ as:

$$(\vec{\mathbf{P}})_i = (e)_{ijk}(\vec{\varepsilon})_{jk} \quad (4)$$

where the third order tensor $(\mathbf{e})_{ijk}$ is the piezoelectric coefficient tensor. According to the conventional theory of piezoelectric and elasticity, [22,24] the constitutive equations can be written as:

$$\begin{cases} \vec{T} = c_E\vec{\varepsilon} - e^T\vec{E} \\ \vec{D} = e\vec{\varepsilon} + k\vec{E} \end{cases} \quad (5)$$

where $\vec{T}$ is the stress vector, $\vec{E}$ is the electric field vector, $\vec{D}$ is the electric displacement vector, c_E is the elasticity tensor, and k is the dielectric tensor.

For simplicity of illustrating the basic physics, several assumptions were made: one-dimension piezotronic p-n junction was considered for analytical analysis; strain was applied normal to the material interface without introducing shear strain; the p-type region was non-piezoelectric and n-type region was piezoelectric. Considering that ZnO nanostructures grow along the direction of c-axis, positive charges were created at the n-type side of the p-n junction by applying a compressive stress along the c-axis. Rather than conventional surface charge assumption in bulk piezoelectric materials, it was assumed that the piezo-charges distribute at the interface of p-n junction within a width of W_{piezo}, as shown in Fig. 2a.

For doping level, since p-n junction is usually formed by contact of two materials, abrupt junction model was adopted, in which the impurity concentration in a p-n junction changed abruptly from acceptor concentration N_A to donor concentration N_D, as shown in Fig. 2a. The electrons and holes in the junction region form a charge depletion zone, which were assumed to have a box profile. The electric field and potential distribution inside the p-n junction were first calculated. For one-dimensional device, the Poisson Eq. (1) reduced to:

$$-\frac{d^2\psi_i}{dx^2} = \frac{dE}{dx} = \frac{\rho(x)}{\varepsilon_s} = \frac{1}{\varepsilon_s}[qN_D(x) - qn(x) - qN_A(x) + qp(x) + q\rho_{piezo}(x)] \quad (6)$$

where $N_D(x)$ is the donor concentration, $N_A(x)$ is the acceptor concentration, and $\rho_{piezo}(x)$ is the density of polarization charges (in units of electron charge). W_{Dp} and W_{Dn} were defined to be the depletion layer widths in the p-side and the n-side, respectively.

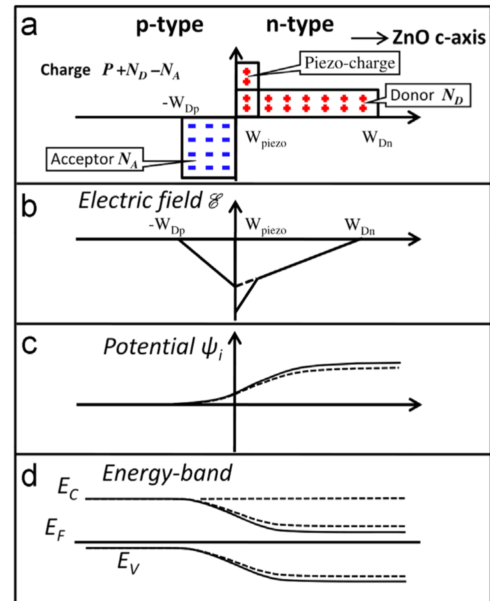

Fig. 2 Piezoelectric p-n junction with the presence of piezo-charges at applied voltage $V=0$ (thermal equilibrium). (a) Piezo-charges, acceptor and donor charges distribution; (b) Electric field, (c) potential distribution and (d) energy band diagram with the presence of piezo-charges. Dashed lines indicate electric field, potential and energy band with the absence of piezo-charges, and the solid lines are for the cases when piezoelectric polarization is present at the n-type side. Reproduced with permission from Wiley [20].

Under small strain condition, the amount of piezo-charge was considered a small perturbation, the depletion width was assumed to be not affected by the existence of piezo-charge, and the resulting phenomenon was the change of built-in potential height. Such assumption gives the most convenient and intuitive analytical result. The electric field intensity was then obtained by integrating the above equations, as shown in Fig. 2b:

$$E(x) = -\frac{qN_A(x+W_{Dp})}{\varepsilon_s}, \text{ for } -W_{Dp} \le x \le 0 \quad (7a)$$

$$E(x) = -\frac{q[N_D(W_{Dn}-x) + \rho_{piezo}(W_{piezo}-x)]}{\varepsilon_s}, \text{ for } 0 \le x \le W_{piezo} \quad (7b)$$

$$E(x) = -\frac{qN_D}{\varepsilon_s}(W_{Dn}-x), \text{ for } W_{piezo} \le x \le W_{Dn} \quad (7c)$$

The maximum field E_m that exists at $\mathbf{x}=0$ was given by

$$\left|\vec{E}_m\right| = \frac{q(N_D W_{Dn} + \rho_{piezo}W_{piezo})}{\varepsilon_s} \quad (8)$$

The potential distribution $\psi_i(x)$ was (as shown in Fig. 2c)

$$\psi_i(x) = \frac{qN_A(x+W_{Dp})^2}{2\varepsilon_s}, \text{ for } -W_{Dp} \le x \le 0 \quad (9a)$$

$$\psi_i(x) = \psi_i(0) + \frac{q}{\varepsilon_s}\left[N_D\left(W_{Dn} - \frac{x}{2}\right)x + \rho_{piezo}\left(W_{piezo} - \frac{x}{2}\right)x\right], \text{ for } 0 \le x \le W_{piezo} \quad (9b)$$

Please cite this article as: Y. Liu, et al., Fundamental theories of piezotronics and piezo-phototronics, Nano Energy (2014), http://dx.doi.org/10.1016/j.nanoen.2014.11.051

$$\psi_i(x) = \psi_i(W_{piezo}) - \frac{qN_D}{\varepsilon_s}\left(W_{Dn} - \frac{W_{piezo}}{2}\right)W_{piezo} + \frac{qN_D}{\varepsilon_s}\left(W_{Dn} - \frac{x}{2}\right)x, \text{ for } W_{piezo} \le x \le W_{Dn} \tag{9c}$$

Thus, the built-in potential ψ_{bi} was given by:

$$\psi_{bi} = \frac{q}{2\varepsilon_s}(N_A W_{Dp}^2 + \rho_{piezo} W_{piezo}^2 + N_D W_{Dn}^2) \tag{10}$$

Eq. (10) presented the change in built-in potential as a result of piezo-charges due to tensile or compressive straining that defines the sign of the local piezo-charges.

Next, the current-voltage characteristics were analyzed for a piezoelectric p-n junction by using the Shockley theory, which modeled an ideal junction based on four assumptions: (i) a piezoelectric p-n junction had an abrupt depletion-layer; (ii) piezoelectric semiconductors was non-degenerate so that the Boltzmann approximation applies; (iii) the injected minority carrier concentration was smaller than the majority carrier concentration so the low-injection assumption for minority carrier was valid; and (iv) no generation-recombination current existed inside the depletion layer, and the electron and hole currents were constant throughout the p-n junction. If the width of the piezo-charges was much less than the width of the depletion zone, for example, $W_{piezo} \ll W_{Dn}$, the effect of piezo-charges on ZnO energy band was considered as a perturbation. The total current density was received by solving Eq. (2): [21]

$$\vec{J} = \vec{J}_p + \vec{J}_n = \vec{J}_0\left[\exp\left(\frac{qV}{kT}\right) - 1\right] \tag{11}$$

where the saturation current $\vec{J}_0 \equiv (q\vec{D}_p p_{n0}/L_p) + (q\vec{D}_n n_{p0}/L_n)$, p_{n0} was the thermal equilibrium hole concentration in n-type semiconductor and n_{n0} was the thermal equilibrium electron concentration in p-type semiconductor, and L_p and L_n were diffusion lengths of electrons and holes, respectively. The intrinsic carrier density n_i was given by:

$$n_i = N_C \exp\left(-\frac{E_C - E_i}{kT}\right) \tag{12}$$

where N_C was the effective density of states in the conduction band, E_i was the intrinsic Fermi level, and E_C was the bottom edge of the conduction band.

For a simple case in which the n-type side had an abrupt junction with donor concentration N_D, and locally $p_{n0} \gg n_{p0}$, $\vec{J}_0 \approx q\vec{D}_p p_{n0}/L_p$, where $p_{n0} = n_i \exp((E_i - E_F)/kT)$, the total current density was given by:

$$\vec{J} = \vec{J}_0\left[\exp\left(\frac{qV}{kT}\right) - 1\right] = \frac{q\vec{D}_p n_i}{L_p}\exp\left(\frac{E_i - E_F}{kT}\right)\left[\exp\left(\frac{qV}{kT}\right) - 1\right] \tag{13}$$

J_{C0} and E_{F0} were defined to be the saturation current density and the Fermi level with the absence of piezo-charges,

$$\vec{J}_{C0} = \frac{q\vec{D}_p n_i}{L_p}\exp\left(\frac{E_i - E_{F0}}{kT}\right) \tag{14}$$

According to Eqs. (9a), (9b), (9c) and (10), the effective Fermi level E_F with the presence of piezo-charges was given by:

$$E_F = E_{F0} - \frac{q^2 \rho_{piezo} W_{piezo}^2}{2\varepsilon_s} \tag{15}$$

Substituting Eqs. (14) and (15) into Eq. (13), current-voltage characteristics was obtained for the piezoelectric p-n junction.

$$\vec{J} = \vec{J}_{C0}\exp\left(\frac{q^2 \rho_{piezo} W_{piezo}^2}{2\varepsilon_s kT}\right)\left[\exp\left(\frac{qV}{kT}\right) - 1\right] \tag{16}$$

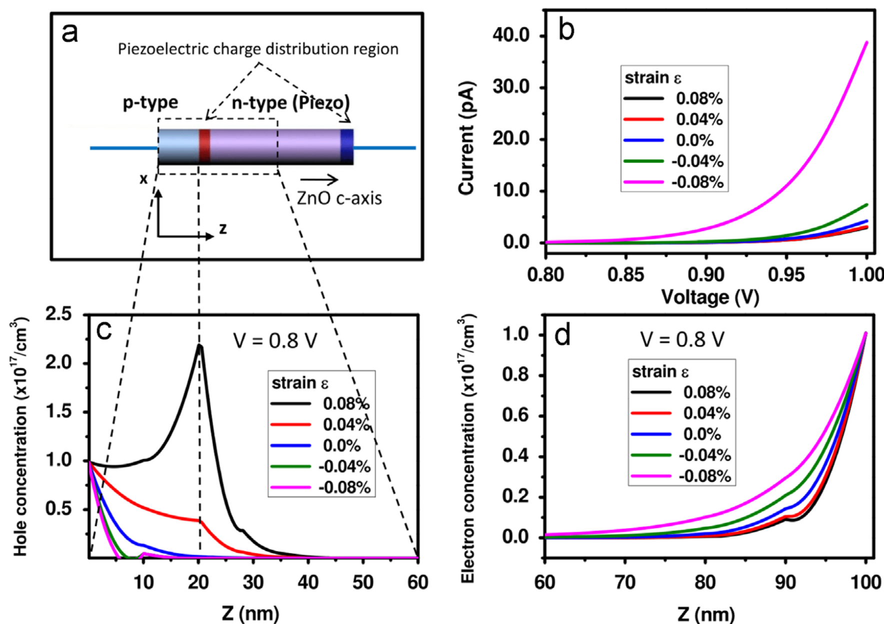

Fig. 3 (a) Schematic of a piezotronic ZnO NW p-n junction; (b) Calculated current-voltage curves, (c) distribution of holes and (d) distribution of electrons at a fixed forward bias voltage of 0.8 V across the p-n junction under various applied strain (−0.09% to 0.09%). Reproduced with permission from Wiley [20].

Please cite this article as: Y. Liu, et al., Fundamental theories of piezotronics and piezo-phototronics, Nano Energy (2014), http://dx.doi.org/10.1016/j.nanoen.2014.11.051

From Eq. (16), it was shown that the current transported across the p-n junction was an exponential function of the local piezo-charges, whereas the sign of piezo-charges depended on the strain. This result was based on the assumptions on ideal cases and simplifications. In real cases, the relationship between current and strain may not be as significant as exponential relationship, yet it was still demonstrated that the current to be transported was effectively tuned or controlled by not only the magnitude of the strain, but also by the sign of the strain (tensile vs compressive).

Simulation of piezotronic P-N junction using finite element method

To demonstrate the generosity and practicality of the piezotronics theory, the basic equations of piezotronic were solved numerically based on the geometry of a typical nanowire (NW) device. Fig. 3a showed a sketch of a piezotronic NW p-n junction to be used for the calculation. The current-voltage characteristics of the p-n junction with uniform strain were studied as a first step. The piezo-charge distribution was received by numerically solving Eqs. (4) and (5). Then the electrostatic equation, the convection and diffusion equations, and continuous equations were solved using the COMSOL software. The electrical contacts at the ends of the p-n junction were set as ideal Ohmic contacts, the Dirichlet boundary conditions were adopted for the carrier concentration and electrical potential at the device boundaries [25].

In order to have a reasonable comparison to a p-n junction diode, the dopant concentration function N was approximately described using Gaussian functions:

$$N = N_{Dn} + N_{Dnmax} e^{-((z-l)/ch)^2} - N_{Apmax} e^{-(z/ch)^2} \quad (17)$$

where N_{Dn} is the n-type background doping concentration due to the presence of intrinsic defects, N_{Dnmax} is the maximum donor doping concentration and N_{Apmax} is the maximum acceptor doping concentration, l is the length of ZnO NW, ch controls the spreads width of the dopant concentration. N is assigned to have a negative value in p-type region and a positive value in n-type region.

For boundaries conditions in contact with a metal electrode, the electrostatic potential was a constant. Infinite recombination velocity was assumed as well as no charge at the contact. Under an applied voltage, the electrostatic potential at the electrode was the potential corresponding to the quasi Fermi level plus the applied voltage V. The electrostatic potential and carrier concentration at the electrode were given by [21,26]:

$$\psi = V + \frac{q}{kT} ln\left(\frac{(N/2) + \sqrt{(N/2)^2 + n_i^2}}{n_i}\right) \quad (18a)$$

$$n = \frac{N}{2} + \sqrt{\left(\frac{N}{2}\right)^2 + n_i^2} \quad (18b)$$

$$p = -\frac{N}{2} + \sqrt{\left(\frac{N}{2}\right)^2 + n_i^2} \quad (18c)$$

In the simulation, ZnO was chosen as the piezoelectric semiconductor material. The length and radius of NW device were 100 nm and 10 nm, respectively. The p-type was assumed non-piezoelectric so it was not restricted to the Wurtzite family. For simplicity, the difference in bandgap between the p-type semiconductor and ZnO was neglected. The length of the p-type was 20 nm and the length of n-type ZnO was 80 nm. The relative dielectric constants are $\kappa^r_\perp = 7.77$ and $\kappa^r_{//} = 8.91$. The intrinsic carrier density is $n_i = 1 \times 10^6\ cm^{-3}$. The electron and hole mobility are $\mu_n = 200\ cm^2/V{\bullet}s$ and $\mu_p = 180\ cm^2/V{\bullet}s$. The carrier lifetimes are $\tau_p = \tau_n = 0.1\ \mu s$. The n-type background doping concentration is $N_{Dn} = 1 \times 10^{15}\ cm^{-3}$. The maximum donor doping concentration is $N_{Dnmax} = 1 \times 10^{17}\ cm^{-3}$ and the maximum acceptor doping concentration is $N_{Apmax} = 1 \times 10^{17}\ cm^{-3}$. The control constant $ch = 4.66$ nm. It was assumed that $W_{piezo} = 0.25$ nm, as represented schematically by red and blue colored zones in Fig. 3a. For easier labeling, z-axis was defined in Fig. 3a, with $z=0$ represents the end of the p-type. The p-n junction is located at $z=20$ nm along the axis. The n-type ends at $z=100$ nm.

The current-voltage curves at various strains were shown in Fig. 3b. For compressive strain, positive piezo-charges assembled at the p-n interface side, resulting in a reduction in built-in potential adjacent to the p-n junction. Thus, the corresponding saturation current density increased at a fixed bias voltage. For tensile strain, negative piezo-charges were created adjacent to p-n interface, resulting in an increase in the built-in potential and dropping in saturation current.

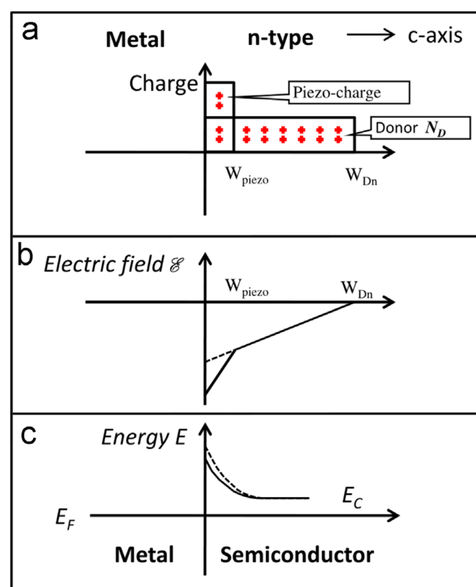

Fig. 4 Ideal metal-semiconductor Schottky contacts with the presence of piezo-charges at applied voltage $V=0$ (thermal equilibrium). (a) Space charges distribution; (b) Electric field and (c) energy band diagram with the presence of piezo-charges. Dashed lines indicate electric field and energy band with the absence of piezo-charges, and the solid lines are for the cases when piezoelectric polarization is present in the semiconductor. Reproduced with permission from Wiley [20].

Please cite this article as: Y. Liu, et al., Fundamental theories of piezotronics and piezo-phototronics, Nano Energy (2014), http://dx.doi.org/10.1016/j.nanoen.2014.11.051

ARTICLE IN PRESS

Analytical theory for metal-semiconductor contact

The metal-semiconductor (M-S) contact is also an important component in electronic devices, especially in NW based sensors. Similar to the analysis to the piezoelectric p-n junction, the M-S contact was simplified in the charge distribution as shown in Fig. 4a with the presence of a Schottky barrier. The semiconductor side was assumed to be n-type, and the surface states and other anomalies were ignored for simplification. Under straining, the created piezo-charges at the interface not only changed the height of the Schottky barrier, but also its width. Different from the method of introducing dopants at the semiconductor side, the piezo-charges can be continuously tuned by strain for a fabricated device.

According to diffusion theory, the carriers transport in M-S contact was dominated by the majority carriers. The current density Eq. (2) can be rewritten as: [21]

$$\vec{J} = \vec{J}_n = q\mu_n n\vec{E} + q\vec{D}_n \frac{dn}{dx} \tag{19}$$

where $E = d\psi_i/dx = dE_c/dx$. The solutions under forward bias (positive bias on metal side) were obtained as: [21]

$$\vec{J}_n \approx \vec{J}_D exp\left(-\frac{q\phi_{Bn}}{kT}\right)\left[exp\left(\frac{qV}{kT}\right) - 1\right] \tag{20}$$

where $\vec{J}_D = q^2 D_n N_C/kT\sqrt{2qN_D(\psi_{bi} - V)/\varepsilon_s}exp(-(q\phi_{Bn}/kT))$ is the saturation current density. J_{D0} was defined as the saturation current density with the absence of piezo-charges:

$$\vec{J}_{D0} = \frac{q^2\vec{D}_n N_C}{kT}\sqrt{\frac{2qN_D(\psi_{bi0} - V)}{\varepsilon_s}}exp\left(-\frac{q\phi_{Bn0}}{kT}\right) \tag{21}$$

where ψ_{bi0} and ϕ_{Bn0} are built-in potential and Schottky barrier height with the absence of piezo-charges. The effect of piezo-charge was again considered as perturbation to the conduction band edge E_C. The change in effective Schottky barrier height induced by piezo-charges was derived from the potential distribution Eqs. (9a), (9b), (9c) and (10):

$$\phi_{Bn} = \phi_{Bn0} - \frac{q^2\rho_{piezo}W_{piezo}^2}{2\varepsilon_s} \tag{22}$$

Thus, the current density was rewritten as:

$$\vec{J}_n \approx \vec{J}_{D0} exp\left(\frac{q^2\rho_{piezo}W_{piezo}^2}{2\varepsilon_s kT}\right)\left[exp\left(\frac{qV}{kT}\right) - 1\right] \tag{23}$$

which is similar to the Eq. (16) for p-n junction. Therefore, the current to be transported was also effectively tuned or controlled by both the magnitude of the strain and the sign of the strain.

For a special case of metal-Wurtzite semiconductor contact, such as Au-ZnO or Ag-ZnO, for the ZnO NW grown along c-axis, the piezocoefficient matrix is written as $(\mathbf{e})_{ijk} = \begin{pmatrix} 0 & 0 & 0 & 0 & e_{15} & 0 \\ 0 & 0 & 0 & e_{15} & 0 & 0 \\ e_{31} & e_{31} & e_{33} & 0 & 0 & 0 \end{pmatrix}$. The applied strain was assumed to be ε_{33} along the c-axis, and piezoelectric polarization was obtained from Eqs. (4) and (5):

$$P_z = e_{33}\varepsilon_{33} = q\rho_{piezo}W_{piezo} \tag{24}$$

The current density was:

$$\vec{J} = \vec{J}_{D0} exp\left(\frac{qe_{33}\varepsilon_{33}W_{piezo}}{2\varepsilon_s kT}\right)\left[exp\left(\frac{qV}{kT}\right) - 1\right] \tag{25}$$

The current transported across the M-S interface was directly related to the exponential of the local strain, meaning the current could tuned on or off by controlling strain.

For numerical calculation, the material constants were: piezoelectric constants e_{33}=1.22 C/m^2, relative dielectric constant ε_S=8.91, width of the piezo-charges W_{piezo}=0.25 nm, temperature T=300 K. Fig. 5(a) showed the calculated J/J_{D0} as a function of the externally applied voltage V across the M-S interface and as a function of the strain, clearly demonstrating its tuning effect on the transported current. When the external voltage was fixed at V=0.5 V at forward bias, J/J_{D0} decreased when the strain changed from -1% to 1% (Fig. 5b). The theoretical result agreed qualitatively with previous experiments [27].

Simulation for a piezoelectric transistor

M-S-M structured ZnO NW devices were the typical piezo-electric transistor used in experimental studies. Using FEM, basic equations was solved for the M-S-M ZnO NW device with the applied strain along the NW length direction (c-

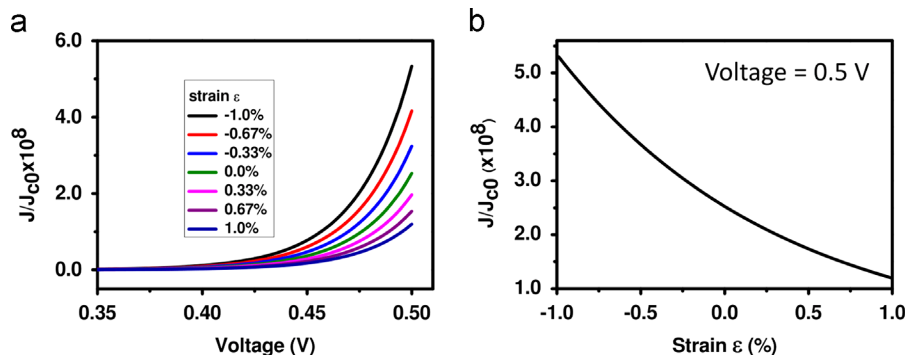

Fig. 5 The current-voltage characteristics of an ideal metal-semiconductor Schottky contact with the presence of piezo-charges. (a) Current-voltage curves at various strain from −1% to 1%; (b) Relative current density as a function of strain at a fixed forward bias voltage of 0.5 V. Reproduced with permission from Wiley [20].

Please cite this article as: Y. Liu, et al., Fundamental theories of piezotronics and piezo-phototronics, Nano Energy (2014), http://dx.doi.org/10.1016/j.nanoen.2014.11.051

ARTICLE IN PRESS

axis). The calculations were done based on a device model with the following device properties assumptions: (i) the surface states in ZnO were ignored; (ii) the electrostatic potential were constants at the end electrodes; (iii) the NW was n-type without p-type doping; (iv) the dopant concentration N was approximately described using a Gaussian function; and (v) at equilibrium, the electron concentration at the metal contact was unaffected by the transported current; (vi) infinite recombination velocity and no charge at the contact. The basic principle also applies to more complex cases, such as different surface states, arbitrary doping profiles and different piezoelectric semiconductor materials, etcetera.

Same as the simulation of p-n junction device, the piezoelectric equations were solved first. Then, the electrostatic equation, the convection and diffusion equations were solved with the piezo-charge distribution provided. The dopant concentration function N was approximately described using a Gaussian function:

$$N = N_{Dn} + N_{Dn\ max} e^{-\left(\frac{z-l}{ch}\right)^2} \quad (26)$$

The boundary conditions of the electrostatic potential at the electrode can be given by:

$$\psi = V - \chi_{ZnO} - \frac{E_g}{2} + \frac{q}{kT} ln\left(\frac{(N/2) + \sqrt{(N/2)^2 + n_i^2}}{n_i}\right) \quad (27)$$

where the electron affinity χ_{ZnO} is 4.5 eV, and its band gap E_g is 3.4 eV.

The DC transport property was calculated for an M-S-M ZnO NW device with the presence of piezo-charges with the applied strain from −0.39% to 0.39%. Fig. 6a showed the sketch of piezotronic ZnO NW device. The current-voltage curves were shown in Fig. 6b. At compressive strain, the positive and negative piezo-charges were at the left-hand and right-hand M-S contacts, respectively, as shown in Fig. 6a, which accordingly lowered and raised the local Schottky barrier heights at the corresponding contacts. When external voltage was applied with the left-hand contact at positive bias, the dominant barrier that dictates the current-voltage curve was the reversely biased contact at the right-hand, at which the local barrier height was raised by piezo-charges. Thus, the transported current was lowered in comparison to the case of strain-free device. Alternatively, under tensile strain and the same biased voltage, by the same token, the *I-V* curve was largely determined by the M-S contact at the right-hand side, which has a lowered barrier height, resulting in an increase in transported current in comparison to the strain-free case. The device displays 'ON' state at 0.39% strain, and is 'OFF' at −0.39% strain. Therefore, the piezoelectric polarization acted similar to the 'gate' voltage to tune the current of piezoelectric transistor at the M-S interface and the device can be switched by switching the applied strain, which was the piezotronic FET.

Theory of piezo-phototronics

Theory for metal-semiconductor structure and application in photodetection [19]

For photodetectors based on a single Schottky or a double Schottky contacted Metal-Semiconductor-Metal (MSM) structures, the most important figure of merit is the responsivity, which is defined as the ratio of photocurrent over the incident

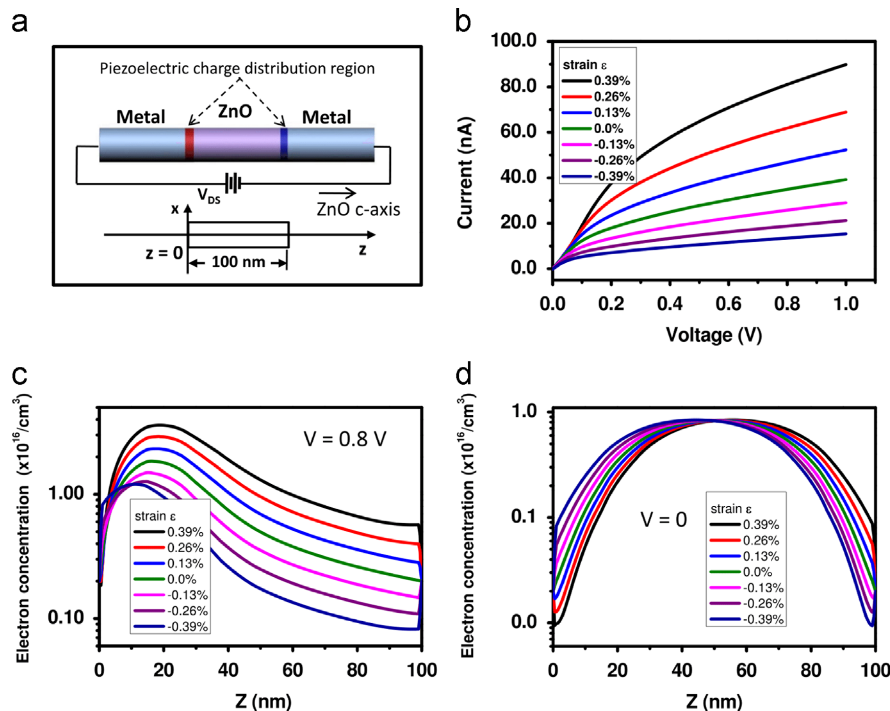

Fig. 6 (a) Schematic of piezotronic ZnO NW transistor. (b) Calculated current-voltage curves of the device at various applied strain (−0.39% to 0.39%); Electron distribution in the semiconductor segment (c) at a forward voltage of V=0.8 V and (d) at V=0. Reproduced with permission from Wiley [20].

Please cite this article as: Y. Liu, et al., Fundamental theories of piezotronics and piezo-phototronics, Nano Energy (2014), http://dx.doi.org/10.1016/j.nanoen.2014.11.051

optical power. Thus, the effect of piezo-phototronics was evaluated by its influence over the photocurrent in the theoretical study. In the theoretical study, photoexcitation and piezoelectric terms were coupled into the basic current equations to study their influence on the final device performance. Besides the fundamental equations used in theory of piezotronics, as shown in Eqs. (1-5), photoexcitation equation should was also considered.

In semiconductor materials with direct band gap, photons with energy higher than the band gap (E_g) of the photodetector material will excite electron-hole pairs. Under a steady light illumination, the excess free carrier concentration is given by the continuity equation [28]

$$\Delta n = \Delta p = \tau_n G_L(I) \tag{28}$$

where Δn is the excess electron concentration and Δp the excess hole concentration under light illumination, τ_n is the carrier lifetime, and $G_L(I)$ is the rate of photon generation, which is a function of light intensity.

Without photoexcitation, the Fermi level of the semiconductor lined up with the Fermi level of the metal. When light is illuminated onto the NW, the existence of excess carriers resulted in a split of the original Fermi level into two quasi-Fermi levels for electrons and holes accordingly, as shown in Fig. 7b. In bulk materials, the absorption of light decayed with distance into the semiconductor, yet in NW photodetector, as the NW diameter is so small, it is reasonable to assume that as long as light illumination is uniform, the quasi Fermi level should also be uniform along the entire NW. The quasi Fermi level E_{Fn} for electrons and E_{Fp} for holes can be described by [21]

$$E_{\mathrm{F_n}} = E_{\mathrm{F}} + kT \ln\left(\frac{n_0+\Delta n}{n_0}\right) \tag{29}$$

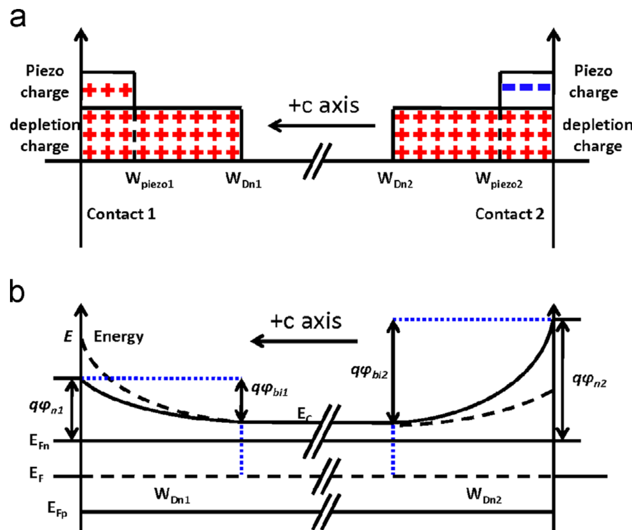

Fig. 7 Illustration of ideal metal-semiconductor-metal structures with the presence of piezo-charges and photon generated charges. (a) Space charge distribution and corresponding (b) energy band diagram in the presence of piezo-charges and photo generated charges. Dashed lines stand for original barriers without strain nor photoexcitation. The solid line is the finally tuned band structure by the piezo-charges, with one end being lifted up and one side being lowed. Reproduced with permission from Wiley [19].

$$E_{\mathrm{Fp}} = E_{\mathrm{F}} - kT \ln\left(\frac{p_0+\Delta p}{p_0}\right) \tag{30}$$

Current density for forward biased and reversely biased Schottky contact

For a n-type Schottky contacted device between a metal and a semiconductor, under forward bias voltage, the thermionic emission (TE) theory was adopted for the charge carrier transport, and the current density under forward bias J_{F} is [21]

$$J_{\mathrm{F}} = A^* T^2 e^{-(q/kT)\phi_n}\left(e^{(q/kT)V} - 1\right) \tag{31}$$

where A^* is the Richardson constant, T is temperature, ϕ_n is the effective Schottky barrier height, and V is the applied voltage across the contact.

For a reversely biased n-type Schottky contact, the thermionic field emission (TFE) theory better described the behavior of heavily doped semiconductor materials with considering the tunneling effect [21,29]. According to the TFE theory, the current density under reverse bias took the form of

$$J_{\mathrm{R}} = J_{\mathrm{sv}} e^{-(q/E_0)\phi_n} e^{V_{\mathrm{R}}((q/kT)-(q/E_0))} \tag{32}$$

where J_{sv} was the slowly varying term regarding applied voltage and Schottky barrier change, V_{R} was the reverse voltage, k the Boltzmann constant, and E_0 was a tunneling parameter of the same order of but larger than kT [30]. Usually E_0 was larger than kT, and was constant regarding barrier height and applied voltage, so it was reasonable to assume that $E_0 = akT$, with $a > 1$, and Eq. (32) now becomes

$$J_{\mathrm{R}} = J_{\mathrm{sv}} e^{-(q/akT)\phi_n} e^{V_{\mathrm{R}}(q/kT)(1-(1/a))} \tag{33}$$

Piezo-phototronics effect for a single Schottky contact

Same as in the theoretical frame work for piezotronics, the modification to the Schottky barrier height by piezo-charges was

$$\Delta\phi_{\mathrm{piezo}} = -\frac{1}{2\varepsilon}\rho_{\mathrm{piezo}} W_{\mathrm{piezo}}^2 \tag{34}$$

For a Schottky contact, photo excitation and introduction of local piezo-charges could change the barrier height, which was quantitatively expressed as

$$\Delta\phi_n = -\frac{1}{2\varepsilon}\rho_{\mathrm{piezo}} W_{\mathrm{piezo}}^2 - \frac{kT}{q}\ln\left(\frac{n_0+\Delta n}{n_0}\right) \tag{35}$$

Thus, the modified barrier height was

$$\phi_n = \phi_{\mathrm{Bn0}} + \Delta\phi_n \tag{36}$$

The electron current density transported through a forwardly biased Schottky contact was then

$$J_n = J_{n0}\left(\frac{n_0+\Delta n}{n_0}\right)\exp\left(\frac{q}{kT}\frac{1}{2\varepsilon}\rho_{\mathrm{piezo}} W_{\mathrm{piezo}}^2\right) \tag{37}$$

where J_{n0} was the current density without applying light illumination nor external strain, and $J_{n0} = A^* T^2 e^{-(q/kT)\phi_{\mathrm{Bn0}}}\left(e^{(q/kT)V} - 1\right)$

As the sign of ρ_{piezo} depends on the direction of c-axis and type of applied strain, the influence of piezo-charges could either enhance photo excitation or reduce it.

Please cite this article as: Y. Liu, et al., Fundamental theories of piezotronics and piezo-phototronics, Nano Energy (2014), http://dx.doi.org/10.1016/j.nanoen.2014.11.051

Piezo-phototronics effect for a double-Schottky-contact structure

As piezoelectricity originated from inner crystal polarization of ions, the piezo-charges could be seen as fixed charges at the two ends of the NW with opposite signs, which was shown in Fig. 7a. For a Wurtzite structured NW with strain along the c-axis, which was assumed to be the growth direction of the NW, the piezo polarization was

$$P = e_{33}\varepsilon_{33} = \rho_{\text{piezo1}} W_{\text{piezo1}} = -\rho_{\text{piezo2}} W_{\text{piezo2}} \tag{38}$$

where ε_{33} stood for the strain along the c-axis, ρ_{piezo1} was the density of the strain-induced piezo-charges at contact 1, and ρ_{piezo2} was the density of the strain-induced piezo-charges at contact 2.

In a device with double Schottky contacts, with certain bias voltage, one junction would be reversely biased and the other junction would be forwardly biased. The current across the double Schottky junction device should take the form

$$I = S_R J_R = V_{NW}/R_{NW} = S_F J_F \tag{39}$$

where S_R and S_F were cross section area for reverse junction and forward junction accordingly, R_{NW} was the resistance of the NW, and V_{NW} was the voltage across the NW. Thus

$$V_R + V_{NW} + V_F = V \tag{40}$$

where V_R and V_F were the voltage across the reverse and forward junction, V was the total applied voltage.

In Eq. (39), the R_{NW} term mainly influenced the current behavior at applied voltage above 5 V or higher, [30] and at working voltage range for photodetection, the dominating term should was mainly controlled by the reversely biased contact. To clearly see the effect of piezo-charges and photo excitation, reasonable simplifications were made that $V_R = cV$, where c was assumed constant and $c < 1$. Thus, the total current was expressed as

$$J = J_{sv}\exp\left(-\frac{q}{akT}\phi_{n0}\right)\exp\left[V\frac{q}{kT}c\left(1-\frac{1}{a}\right)\right]\left(\frac{n_0+\Delta n}{n_0}\right)^{1/a} \times\exp\left(\frac{q}{akT}\frac{1}{2\varepsilon}\rho_{\text{piezo}}W_{\text{piezo}}^2\right) \tag{41}$$

Thus, the device current under different bias voltage took the form

$$I = S_1 J_{C1}\left(\frac{n_0+\Delta n}{n_0}\right)^{1/a}\exp\left(\frac{q}{akT}\frac{1}{2\varepsilon}\rho_{\text{piezo1}}W_{\text{piezo1}}^2\right)$$
when contact 1 was under reverse bias ($V > 0$) (42a)

$$I = -S_2 J_{C2}\left(\frac{n_0+\Delta n}{n_0}\right)^{1/a}\exp\left(\frac{q}{akT}\frac{1}{2\varepsilon}\rho_{\text{piezo2}}W_{\text{piezo2}}^2\right)$$
when contact 2 was under reverse bias ($V < 0$) (42b)

where $J_{C1} = J_{sv1}\exp(-(q/a_1 kT)\phi_{n10})\exp[V(q/kT)c_1(1-(1/a_1))]$, and $J_{C2} = J_{sv2}\exp(-(q/a_2 kT)\phi_{n20})\exp[V(q/kT)c_2(1-(1/a_2))]$, were the currents under reverse bias for contact 1 and 2 accordingly, and S_1 and S_2 were the areas for junction 1 and 2, respectively. As ρ_{piezo1} and ρ_{piezo2} had opposite signs, Eqs. (42a) and (42b) showed asymmetric change in photocurrent under opposite bias by the same amount of applied strain.

Numerical calculation of MSM photodetector

For easy comparison with experimental results, the analytical result was applied for numerical calculation for Ag-CdS-Ag structure based visible light detector and Ag-ZnO-Ag structure based UV light detector. For an Ag-CdS-Ag structure with one Ohmic contact and one Schottky contact, when forward bias was applied on the Schottky contact, using Eq. (37), the photocurrent was calculated under the same intensity of light illumination with applied strain varying from 0 to 1%. Depending on the direction of c-axis, the photocurrent could either increase or decrease with applied strain. Fig. 8a and b showed the performance of two single-Schottky-contact devices, the configuration of which were shown in the inset of Fig. 8a and b accordingly. For CdS NW, the dielectric constant $\varepsilon_r = 9.3$,[31] and piezoelectric coefficient $e_{33} = 0.385\ \text{C/m}^3$. For photoexcitation, the external quantum efficiency was assumed as $\eta_{ext} = 1$, the internal gain $\Gamma_G = 1.5\times10^5$, [10] carrier lifetime $\tau_n = 3$ ns. [32] The diameter of the NW was assumed to be 100 nm. At dark condition, electron concentration in NW was assumed as $1\times10^{15}\ \text{cm}^{-3}$.

The photocurrent under strain free condition with different illumination power were calculated as shown in Fig. 8c, which also gave reference to the fluctuation of light

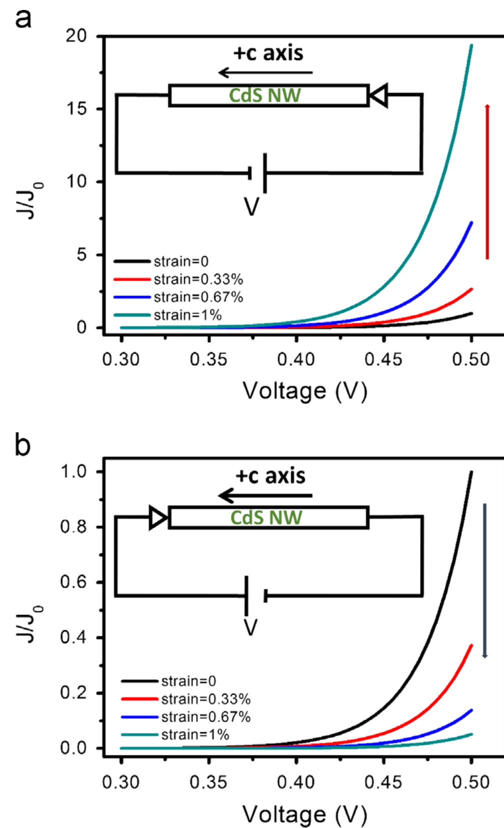

Fig. 8 Results for numerical simulation for a metal-CdS-metal photodetector. J_0 is set as the current of the device at zero strain and at applied voltage of 0.5 V. Insets are the configuration of device and direction of forward bias. (a, b) with a Schottky contact on one end and Ohmic contact on the other end. Relative current density vs. voltage under different strains and the same illumination power, for two devices with different orientation of c-axis regarding the position of the Schottky contact. Reproduced with permission from Wiley [19].

Please cite this article as: Y. Liu, et al., Fundamental theories of piezotronics and piezo-phototronics, Nano Energy (2014), http://dx.doi.org/10.1016/j.nanoen.2014.11.051

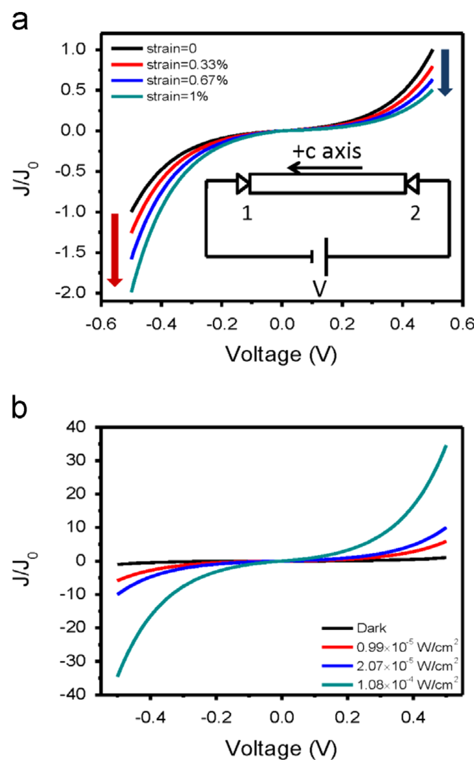

Fig. 9 Numerical simulation for a metal-CdS-metal photodetector with Schottky contact on both ends based on our analytical solution. (a) Relative current density vs. voltage under different strains and the same illumination power. J_0 is set as the current of the device at zero strain and at reverse applied voltage of 0.5 V. Inset is the configuration of device and direction of forward bias. (b) current-voltage diagram under different illumination power. J_0 is set for the dark current at forward applied voltage of 0.5 V. Reproduced with permission from Wiley [19].

intensity in photocurrent measurement. For an Ag-CdS-Ag structure with two Schottky contacts at both ends, it was assumed that a=1.3 and c=0.8 in Eq. (41), which were reasonable values according to previous reports.[30] The result of simulation according was shown in Fig. 9a. The asymmetric characteristic of the piezo-phototronic effect was demonstrated very clearly: the change of current under the same amount of applied strain was opposite when the bias voltage was applied at opposite direction.

For ZnO, the dielectric constant ε_s=8.9, piezoelectric coefficient e_{33}=1.22 C/m^3, carrier lifetime τ_n=3.0 ns [32] which means that the simulation results for ZnO will only have slight difference in magnitude with CdS, and will have the same trends of change with strain and light intensity. Numerical simulation for ZnO photodetection was also carried out and shown in Fig. 10.

Effect of piezoresistance, series resistance and other factors

There are a lot of factors causing deviation of *I-V* characteristic from ideal current-voltage equation. The deformation of crystal lattice under strain can result in a minor change of the band gap width, and can finally result in conductance change of the semiconductor. This is called piezoresistance effect [33,34]. The piezoresistance effect is present in semiconductors either with or without piezoelectricity. In piezotronics and piezo-phototronics, piezoresistance is always accompanied with the piezoelectric effect.

In piezoresistance effect, the change of resistance was given by

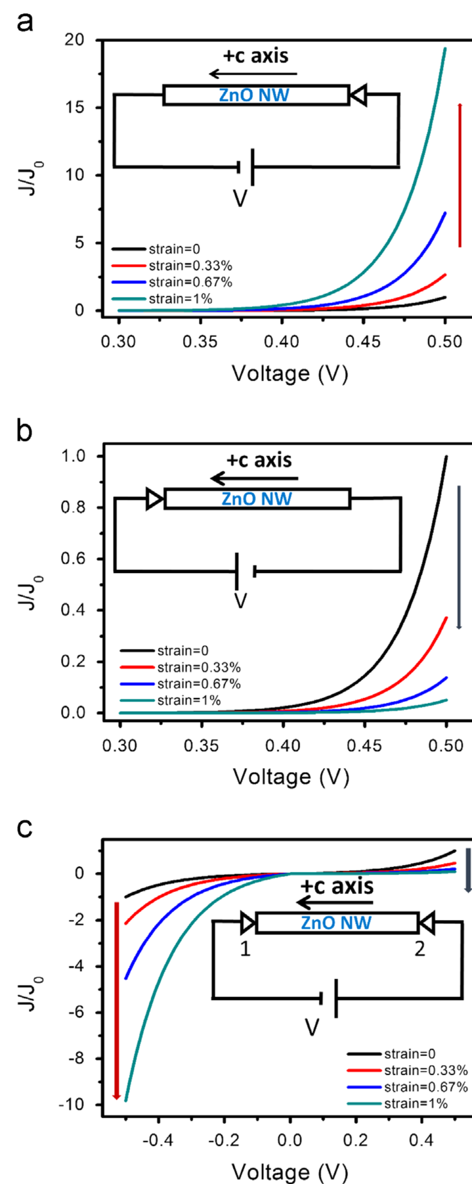

Fig. 10 Numerical calculation regarding photodetection of Ag-ZnO-Ag structure. (a) (b) are relative current density vs. voltage under different strains and the same illumination power, for two devices with different orientation of c-axis regarding the position of the Schottky contact. J_0 is set as the current of the device at zero strain and at applied voltage of 0.5 V. Insets are the configuration of device and direction of forward bias. (c) Relative current density vs. voltage under different strains and the same illumination power. J_0 is set as the current of the device at zero strain and at reverse applied voltage of 0.5 V. Inset is the configuration of device and direction of forward bias. The asymmetric change of current under changing strain is clearly demonstrated. Inset is the change of responsivity for forward bias under positive strain. Reproduced with permission from Wiley [19].

Please cite this article as: Y. Liu, et al., Fundamental theories of piezotronics and piezo-phototronics, Nano Energy (2014), http://dx.doi.org/10.1016/j.nanoen.2014.11.051

ARTICLE IN PRESS

$$\frac{\delta\rho}{\rho} = \pi\frac{\delta l}{l} \quad (43)$$

where ρ was the resistance of the semiconductor, l was the original length of the NW, $\delta\rho$ was the resistance change due to piezoresistance effect, δl was the change in NW length, and π was the piezoresistance coefficient. From Eq. (43), the piezoresistance was shown as a resistance effect that was a uniform and symmetric and volume effect regardless the bias direction of the applied voltage.

Another important factor should be the effect of outer series resistance. Series resistance is the equivalent resistance of various factors in the electric circuit, including outer circuit resistance, capacitors and inductors. Methods to solve the influence of series resistance had been extensively developed [35,36]. According to these solutions, when applied voltage was small, the device behavior was dominated by current equations for contact junction; when applied voltage was large, the device behavior was mostly linear.

Other factors included the surface trapped charges on the contact areas, and change in contact areas due to externally applied strain. These factors either had similar behavior with piezoresistance effect or should be too small to affect the results.

Judging criteria for piezo-phototronic photodetection

According to the nature discovered in piezo-phototronics effect and its discussed difference with non-piezoelectric effects, three criteria were proposed for piezo-phototronic effect for a better understanding of the basic mechanism and its connection to the application in devices.

a) Piezo-phototronic photodetection requires the presence of charge barrier, including a Schottky junction, p-n junction or some special heterostructure [37]. The piezo-charges originate from the dipole nature of piezoelectricity, and they accumulate at the ends of the piezoelectric semiconductor NW in the form of inner crystal fixed charges. With the existence of a charge barrier, the small amount of piezo-charges can effectively tune the current transport properties of the photodetector.
b) Photoexcitation influences the current-voltage characteristic through generating excess free charges. Provided that the entire device is under uniform illumination, photon generation of electrons and holes effectively tunes quasi Fermi level, and this change is applied along the entire wire, resulting in a decrease of the barrier height.
c) Piezoelectric effect influences photodetection by strain induced polar charges at the ends of the NWs. The effect of piezo-charges in a double Schottky contact photodetector shall result in asymmetric change in barrier heights at the two sides. Other factors induced by external strain such as piezoresistance or contact area change will induce symmetric change in both ends of the NW. In this way, we can easily tell whether the change is caused by genuine piezo-phototronics effect.

Theory for p-n junction and application in LEDs and solar cells [18]

p-n junctions are the core structure in LEDs and solar cells. Compared with the relative simple cases in Schottky junctions, piezo-phototronics effect in p-n junction induces much more complicated change in the depletion region, especially when

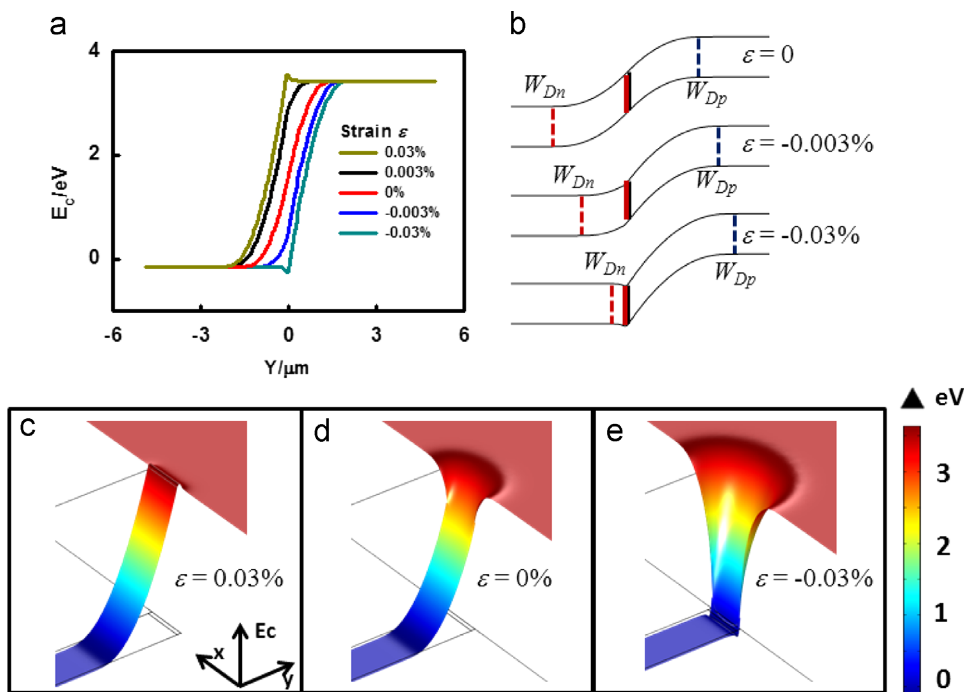

Fig. 11 (a) Conduction band deformation of n-ZnO/p-ZnO structure under different strain on n-type side, 1D simulation, (b) illustration of the formation of charge channel, (c, d, e) Conduction band in height expression from 2D simulation in n-ZnO/p-ZnO structure under (c) 0.03% strain (d) no strain and (e) -0.03% strain at the n-type side. Reproduced with permission from Wiley [18].

Please cite this article as: Y. Liu, et al., Fundamental theories of piezotronics and piezo-phototronics, Nano Energy (2014), http://dx.doi.org/10.1016/j.nanoen.2014.11.051

ARTICLE IN PRESS

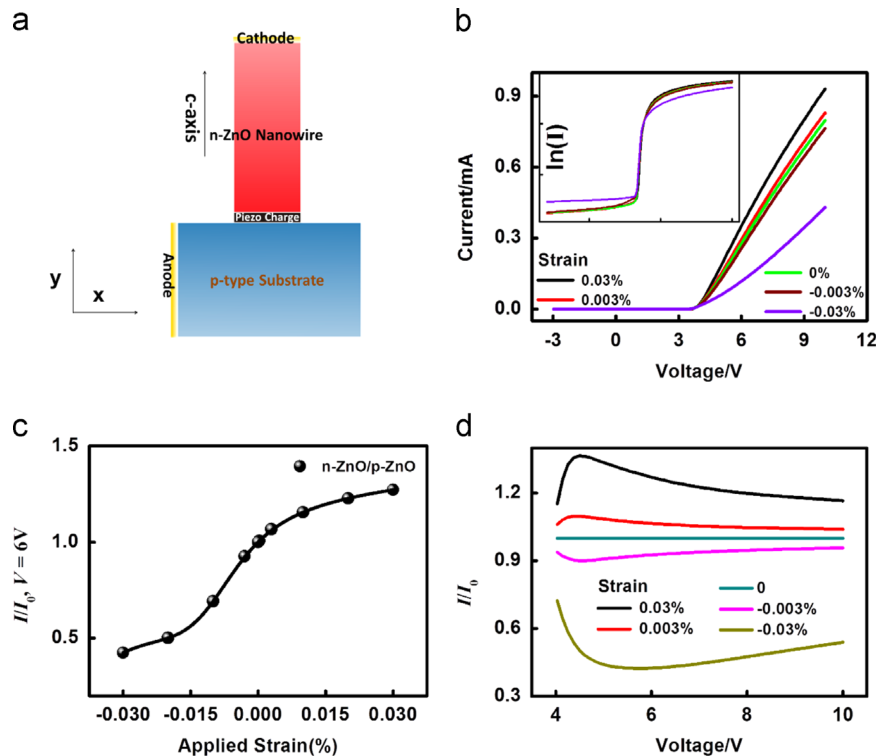

Fig. 12 (a) Geometry of 2D simulation, (b) Current-voltage curve of n-ZnO/p-ZnO, (c) Change of current when bias is fixed at 6 V under different strain, I_{strain}/I_0 vs. ε, (d) Relative change of current under strain vs. applied voltage, I_{strain}/I_0 vs. V. Reproduced with permission from Wiley [18].

the device is composed of NW and thin film with comparable geometric size as the depletion length itself. Under such case, analytical results will be too complicated to give intuitive indication of the working mechanism of piezo-phototronics, and simulations will provide more information on how the piezoelectric polarization influences device performance. For p-n junction based piezo-phototronic devices, a series of simulations were then carried out. A methodology was developed for 2D simulation of the piezo-phototronic effect in a p-n junction based LED, which took device geometry into consideration. Simulated results included band structure and device current characteristics under different device geometries. In such a study, the formation of charge channel in the p-n junction area and the shift of depletion region were observed and confirmed for the first time, which provided a deeper insight to the understanding on how piezoelectric polarization influences optoelectronics device performance.

Model development

COMSOL Multiphysics software was utilized for most of the calculations. Higher ordered solvers and mesh refinement were utilized to avoid the singularity and convergence failure caused by large gradient in charge carrier concentrations. The 2D layout of the theoretical model was built according to common experimental designs, [13,38] including an n-type piezoelectric NW structure and a thin film p-type substrate, as shown in Fig. 12a. The NW was 1 μm × 10 μm and the substrate 10 μm × 10 μm in size. The diameter of the NW was close to the ZnO NW used in LED experiments. One end of the NW was set as the cathode with an ohmic contact while the other end was attached to the surface of a p-type thin film which also supported the NW. The c-axis of the NW was its growth direction, and was set pointing from the substrate to the cathode. Uniaxial strain was applied along the axis of the NW, and the strain-induced piezoelectric polarization charges existed at the p-n junction. The piezo-phototronic effect under both tensile strain and compressive strain were studied. For a p-type NW/n-type thin film structure, the simulated results can be amended to apply without any subtle change. ZnO was utilized as the material for both the n-type NW and the p-type substrate of homojunctions, and p-GaN was utilized to investigate the effect of p-n heterojunctions [39]. The basic material parameters of ZnO/GaN are taken from the database provided with the COMSOL software and from reported data [40,41] as:

Based on the low defect concentration of high temperature chemical vapor deposition (CVD) synthesized ZnO NWs, the doping profile of ZnO was set as $1 \times 10^{15}\ \text{cm}^{-3}$ for both n-type and p-type in the simulation. For a simplified model of the phenomenon, the p-type thin film is assumed non-piezoelectric, and factors including spontaneous polarization, deformation potential and reverse piezoelectric effect were neglected.

Results for numerical simulation

Strain-induced change in band structure. A critical concept in the piezo-phototronics effect was the formation of a channel in the p-n junction region induced by piezo-charge, which effectively tuned the carrier separation or recombination. In reported LED experiments, a positive charge channel

Please cite this article as: Y. Liu, et al., Fundamental theories of piezotronics and piezo-phototronics, Nano Energy (2014), http://dx.doi.org/10.1016/j.nanoen.2014.11.051

ARTICLE IN PRESS

was proposed for trapping the holes in the valence band at the metallurgical junction and increasing the recombination probability, [8] resulting in enhancement of light emission efficiency. Thus, the band structure under strain was calculated and proved this assumption.

The piezo-charge density was obtained from the piezoelectric polarization P, which was retrieved from the constitutive equation, as addressed in Eq. (24). P is first calculated assuming the piezoelectric material was an insulator, polarization charges at the interface area were then obtained and used as input for the next step.

Next, using a 1D FEM model, the band edge deformation under different strain conditions were calculated, and the resulting conduction band is shown in Fig. 11b for a homojunction. The spatial variation of the valence band edge was identical to the spatial variation of the conduction band (offset by the band gap energy). The deformation of the valence band edge and the conduction band edge were calculated by solving the Poisson equation [43]. The electron concentration n and hole concentration p are solved self-consistently in the depletion region.

In regions far from the depletion zone, the conduction band energy and valence band energy were flat and fixed at values calculated from the bulk material properties and the background doping profile. Therefore, built-in potential ψ_{bi} was fixed at the difference between Fermi levels of the original doping. When piezo-charges are present, a 1D approximation resulted in

$$N_A W_{Dp} = N_D W_{Dn} + \rho_{piezo} W_{piezo} \tag{44}$$

N_A was the p-type doping density in the p-type region, N_D was the n-type doping density in the n-type region, W_{Dp} was the depletion width in the p-type region, and W_{Dn} was the depletion width in the n-type region.

Thus, the depletion region will shrink on the n-type side and expand on the p-type side when $\rho_{piezo} > 0$ (positive piezo-charges), as shown in Fig. 11a at strain $\boldsymbol{\varepsilon} = -0.003\%$; when $\rho_{piezo} < 0$ (negative piezo-charges), the depletion region will expand on the n-type side and shrink on the p-type side, as shown in Fig. 11a at $\boldsymbol{\varepsilon} = +0.003\%$.

It was assumed in analytical models that the depletion region would have negligible change in width under strain, and the influence of piezo-charges was mainly changing the local built-in potential. As both the density and total amount of piezo-charges only depended on piezoelectric coefficient of the material and the existing strain, and independent of the doping profile of the material, this assumption was valid when the doping profile was low so that the total amount of depletion charges of the unstrained structure was far greater than the total amount of piezo-charges. Referring to experiments, this assumption was applicable to hydro-thermally grown NWs with abundant defects as well as photodetectors and solar cells with photo excited free charge carriers, [43,44] as depletion charge amount in these materials were far larger than piezo-charges under experimental straining conditions. In devices with low doping profile, the total amount intrinsic depletion charge was much smaller than the amount of piezo-charges at the junction interface, the presence of piezo-charges resulted in significant change to the width and shape of the depletion zone due to the electrostatic interaction.

When the total amount of piezo-charges further increased and $\rho_{piezo} W_{piezo} \gg N_D W_{Dn}$, as shown in Fig. 11b, the entire depletion region shifted toward the p-type region; W_{Dn} shrunk to the width of the piezo-charges distribution, and the localized piezo-charges affected the charge redistribution, and $\Psi_n + \Psi_p > \psi_{bi}$, where Ψ_n was the built-in potential of the n-type side and Ψ_p is the built-in potential of the p-type side. The local deformation will result in the presence of a charge channel, that is, electron trap at $\boldsymbol{\varepsilon} = -0.03\%$ and hole trap at $\boldsymbol{\varepsilon} = +0.03\%$ shown in Fig. 11a.

Next, the 2D geometry in Fig. 12a was simulated, in which case the Poisson equation was written as

$$\begin{cases} \varepsilon_r \left(\frac{\partial E_x}{\partial x} + \frac{\partial E_y}{\partial y} \right) = -qN_A \\ \frac{\partial^2 \Psi_i}{\partial x^2} + \frac{\partial^2 \Psi_i}{\partial y^2} = \frac{qN_A}{\varepsilon_r} \end{cases} \quad \text{on p} - \text{side depletion region} \tag{45a}$$

$$\begin{cases} \varepsilon_r \left(\frac{\partial E_x}{\partial x} + \frac{\partial E_y}{\partial y} \right) = qN_D \\ \frac{\partial^2 \Psi_i}{\partial x^2} + \frac{\partial^2 \Psi_i}{\partial y^2} = -\frac{qN_D}{\varepsilon_r} \end{cases} \quad \text{on n} - \text{side depletion region} \tag{45b}$$

$$\begin{cases} \varepsilon_r \left(\frac{\partial E_x}{\partial x} + \frac{\partial E_y}{\partial y} \right) = q\rho_{piezo} \\ \frac{\partial^2 \Psi_i}{\partial x^2} + \frac{\partial^2 \Psi_i}{\partial y^2} = -\frac{q\rho_{piezo}}{\varepsilon_r} \end{cases} \quad \text{in piezo} - \text{charge region} \tag{45c}$$

2D height plots were shown in Fig. 11c, d, e to demonstrate the change in conduction band structure in the 2D case. In regions close to the middle line on y-axis, $\partial E_y / \partial y$ and $\partial^2 \Psi_{bi} / \partial y^2$ was close to zero, and the result was similar to 1D simulation, charge channel formed at same amount strain. In other parts of the depletion zone, the influence of the piezo-charges decreased compared to the 1D simulation, meaning that the charge channels will require greater strain to become significant, forming a semicircle in the p-type depletion region.

Simulation of current-voltage characteristics. The current-voltage characteristics were among the most important data for piezotronics and piezo-phototronics. Thus, the simulation results for n-ZnO/p-ZnO structure with the geometry layout shown in Fig. 12a were plotted in Fig. 12. The time-dependent continuity equations for current density (as described in Eq. (3)) were used for current calculation and integration through the whole geometric structure [42].

The depletion region was the main barrier for device current. As the majority holes in p-type substrate has low mobility, they provided a large effective inner series resistance. Under compressed strain condition, the p-type depletion region increased in area and spread out to form a semicircle in the substrate. Current was injected into the substrate along the entire boundary of the depletion region and traveled to the substrate contact. As the area depletion region increased, the current traveled a larger average distance, thereby increased the effective series resistance of the substrate, so the device current decreased. Under tensile condition, the p-type depletion region shrunk and the n-type depletion region enlarged, shrinking the depletion region boundary to the diameter of the NW, and lowering the effective series resistance of the substrate. To support such proposed mechanism, comparison simulations were performed and plotted in Fig. 13. When hole mobility increased to a high value, the influence of strain on current almost diminished. Since the change of resistance and current came

Please cite this article as: Y. Liu, et al., Fundamental theories of piezotronics and piezo-phototronics, Nano Energy (2014), http://dx.doi.org/10.1016/j.nanoen.2014.11.051

ARTICLE IN PRESS

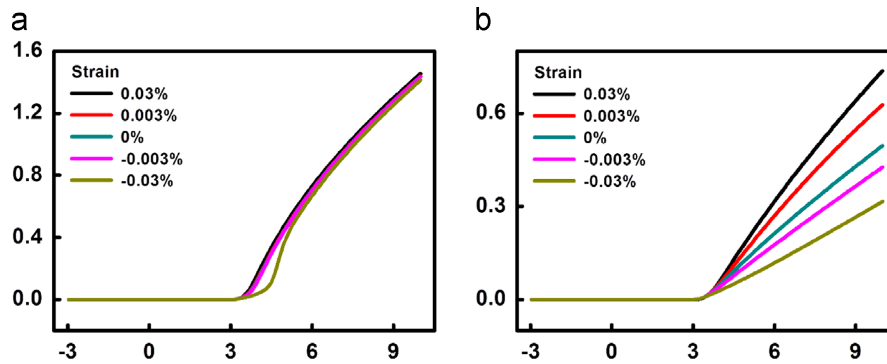

Fig. 13 Current-voltage characteristics under different strain for (a) $\mu_p = 10\ m^2V^{-1}s^{-1}$ and $\mu_n = 0.2\ m^2V^{-1}s^{-1}$ in p-type GaN region, which is unrealistically high for hole mobility, and (b) $\mu_p = 5 \times 10^{-4}\ m^2V^{-1}s^{-1}$ and $\mu_n = 0.2\ m^2V^{-1}s^{-1}$ in p-type GaN region. The influence of strain decreases to a great extent, indicating depletion resistance is the major reason for the current change here. Reproduced with permission from Wiley [18].

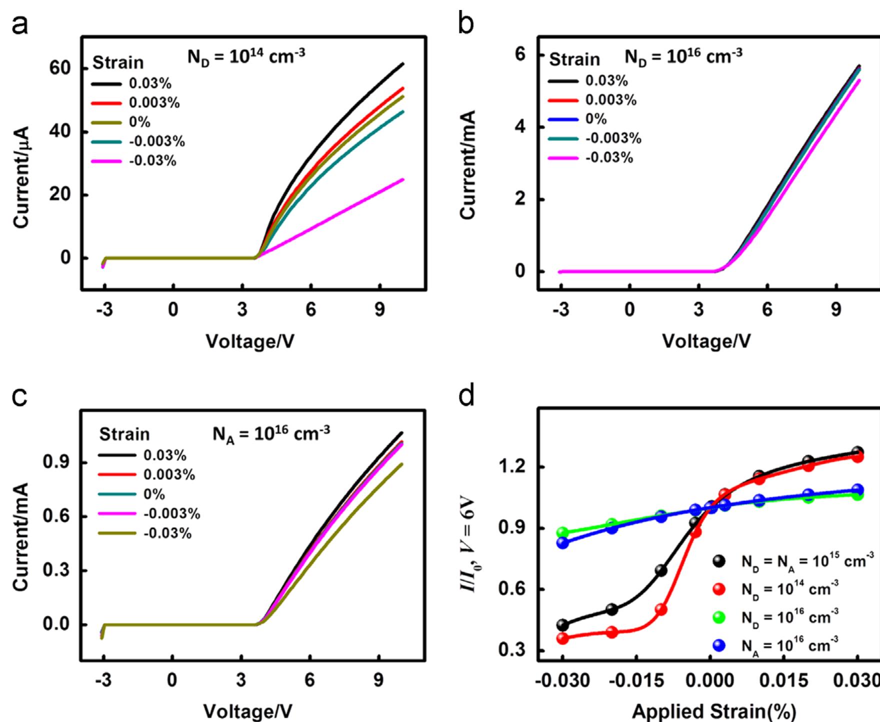

Fig. 14 Current-Voltage simulation result from (a) N_D changes to $10^{14}\ cm^{-3}$, (b) N_D changes to $10^{16}\ cm^{-3}$, (c) N_A changes to $10^{16}\ cm^{-3}$, (d) Comparison of calculated current at a fixed bias of 6 V for different doping concentrations by normalizing to the result received for $N_D = N_A = 10^{15}\ cm^{-3}$. Reproduced with permission from Wiley [18].

from the change of depletion area caused by the introduction of piezo-charges, this change in effective series resistance was totally different from piezoresistance effect or contact area effect. This analysis was consistent to the *I-V* curves under different straining conditions are plotted in Fig. 12b. A monotonic increase in current with increasing tensile strain and decreasing compressive strain was clearly shown. For more intuitive understanding, the current at 6 V under each straining condition were plotted into one curve in Fig. 13c. It was concluded that under lower strain, the current changes almost exponentially with strain; under higher strain, the current saturated when p-channel or n-channel formed at the interface. In Fig. 13d, another comparison was made for the relative change in current I_{strain}/I_0 under different bias voltage for each strain condition. The value of I_{strain}/I_0 at any strain first increased quickly with *V*, and when *V* gets higher, I_{strain}/I_0 finally saturated. When *V* and ε were small, the trend of $I_{strain}/I_0 - V$ and $I_{strain}/I_0 - \varepsilon$ were close to exponential, these results agreed well with analytical models in which exponential relationships between $I_{strain}/I_0 - V$ and $I_{strain}/I_0 - \varepsilon$ were predicted under ideal condition. When *V* and ε gets larger, the $I_{strain}/I_0 - V$ and $I_{strain}/I_0 - \varepsilon$ were closer to linear, which also suggests the effect of series resistance as well as other non-ideal factors.

Optimization of piezo-phototronics effect and device design

Based on such simulation methodology, the parameters related to device design, including doping profile, geometry

ARTICLE IN PRESS

size and material choice were investigated. The optimization of the piezo-phototronics effect could be realized according to these studies.

Study of doping profile

The doping profile was coupled with geometric factors and were essential in device design. In NW devices, materials synthesized by different methods usually exhibit different doping profiles, which causes difference in the influence of piezo-phototronics effect. Several sets of simulations were conducted to study the influence of doping, as shown in Figs. 14 and 15. Fig. 14a-c showed the *I-V* curves under different doping profiles over strain range. Fig. 14d plotted the relative change of current I_{strain}/I_0 at 6 V bias for these simulations for easier comparison.

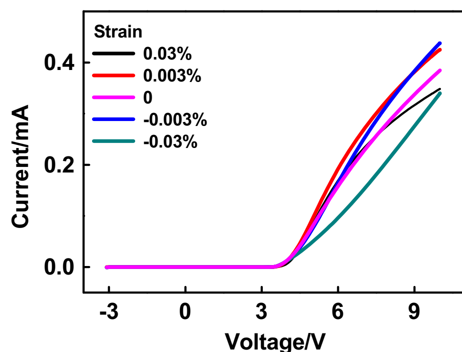

Fig. 15 Current-voltage characteristics under different strain for $N_D=10^{15}\ cm^{-3}$ and $N_A=10^{14}\ cm^{-3}$. Reproduced with permission from Wiley [18].

According to the simulation results, tensile strain still enhanced the current under all doping conditions, but the extent of enhancement varied. Generally, the relative impact of the piezo-phototronic effect decreased when doping profile increased; and the impact of the piezo-phototronic effect increases when doping profile decreases. The mechanism for this influence of doping profile is that the lower the doping profile, the greater the ratio of piezo-charge over depletion charges, thus the more significant the piezo-phototronic effect. This result agreed with the experimental observation that piezo-phototronic effect attenuated in photodetection experiments when detected light intensity increased [10,45]. When detected light intensity increased, the electron-hole pairs generated overwhelmed the influence of piezo-charges.

On the other hand, when the substrate doping reduced to $10^{14}\ cm^{-3}$ while the NW doping stayed the same, the trend of I_{strain}/I_0 under different strain became unsteady, as shown in Fig. 15. There were multiple reasons for such behavior. With lower substrate doping, the depletion region on the p-type side increased in size. From 1D simulation, decreasing the doping profile to 10% of original value increased depletion length by 10 times when no strain is applied. From 2D simulation, in the direction perpendicular to material interface, the change of depletion region was close to the change in 1D simulation; and along the direction parallel to material

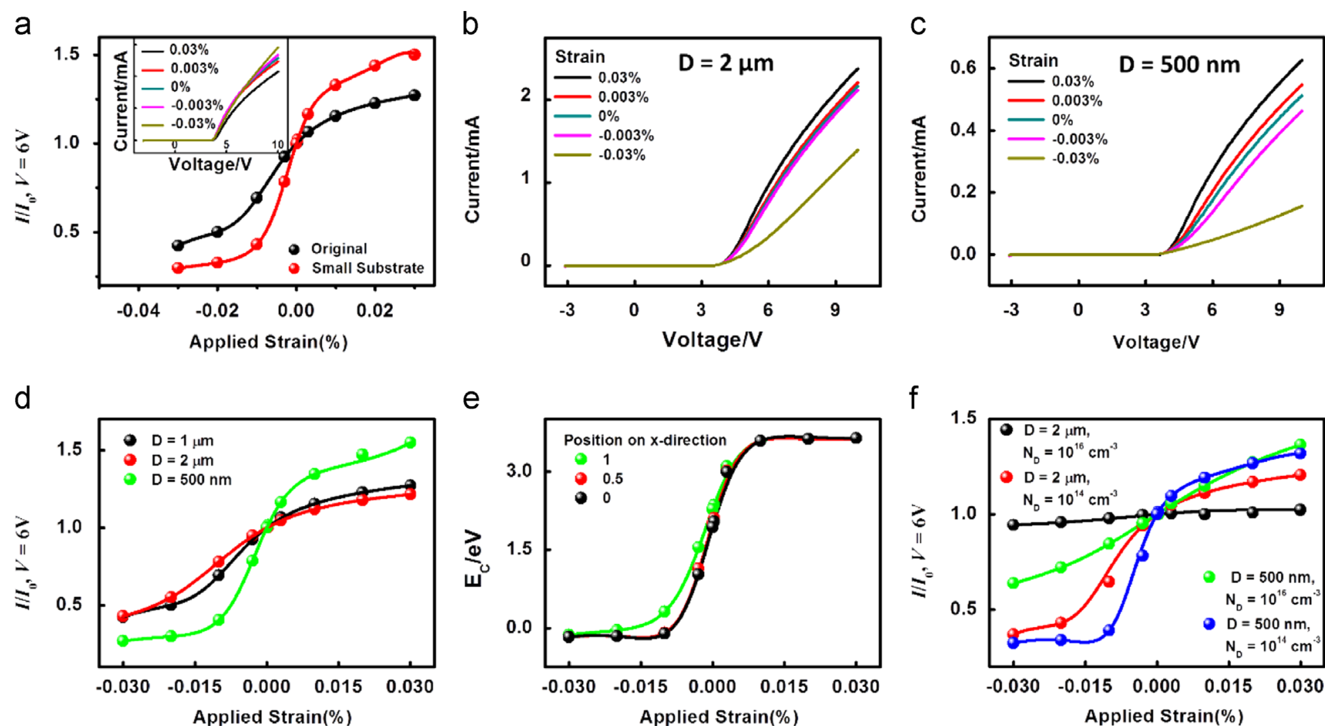

Fig. 16 (a) Comparison of n-ZnO/p-ZnO with smaller substrate of size 5 μm × 5 μm and result in Fig. 2, I_{strain}/I_0 vs. ε at 6 V bias, inset is the current-voltage characteristics of such simulation, (b) current-voltage characteristics of n-ZnO/p-ZnO with NW diameter $D=2$ μm, (c) current-voltage characteristics of n-ZnO/p-ZnO with NW diameter $D=500$ nm, (d) Comparison of I_{strain}/I_0 vs. V, between Fig. 16b, c with Fig. 14c, (e) the E_C value under different strain for different locations along the direction parallel to material interface, position on *x*-direction is counted from the middle point in the piezo-charge distribution area, (f) relative change of current under different NW size and NW doping. Reproduced with permission from Wiley [18].

Please cite this article as: Y. Liu, et al., Fundamental theories of piezotronics and piezo-phototronics, Nano Energy (2014), http://dx.doi.org/10.1016/j.nanoen.2014.11.051

ARTICLE IN PRESS

interface, the change of depletion region was smaller than that in 1D simulation. When the p-type depletion region was large enough to interact with the electrode, it was cut off in the electrode area, and influence of piezo-charges on band structure was much more complicated. Therefore, the device current will also be influenced by both change in band structure and the effective inner resistance created within the depletion region and became unsteady.[46] Thus, piezo-phototronic effect is optimized at certain doping profiles neither too high nor too low. The specific optimized also depended on material properties.

Influence of geometric size. In bulk materials, the device size was usually orders of magnitude greater than the depletion width, and the electrode outlet was usually far away from the depletion region, the size or geometric layout usually influenced the device performance only by influencing the equalized series resistance of the material. However, in NW based devices, the size of the devices was easily comparable to the size of the depletion region, and thus their performance was easily affected by geometry size. For example, when the geometry size was small, the depletion region might either be confined in the geometry in certain dimensions, or might overlap with the electrodes.

Simulation results with change of either the NW diameter or the substrate size were carried out and demonstrated in Fig. 16. In Fig. 16a, the substrate size in simulation was cut half in length and half in width for the structure, which meant that the substrate size is $5\ \mu m \times 5\ \mu m$. From comparison with the original model, the relative current change at the same strain of the small device structure was about 20% larger than that of the original structure for all straining conditions. The uniform enhancement under all strain conditions showed that, as far as the simulated strain and applied voltage was concerned, the depletion region did not overlap with the electrodes and induce unsteadiness in current behavior, and such size shrink mainly changed the series resistance.

Fig. 16b shows the result when the NW diamer is doubled to $2\ \mu m$ and Fig. 14c gives the calculation when the NW diameter is cut to 500 nm. The overall comparison of R value for these two structures with the original geometry was plotted in Fig. 16d. Besides inner resistance, this change also came from the fact that, in direction parallel to material interface (x-direction), the change of band structure by strain was weaker than the change perpendicular to material interface (y-direction), and thus the thinner the NW, the stronger the overall piezo-phototronics effect. For verification, Fig. 16e plotted the E_C value under different strain for different points along the direction parallel to material interface (x-direction), the y value for these points are in the middle of the piezo-charge distribution area. From an optimization aspect, as ZnO was non-ferroelectric, there is no such concept of domains as in PZT or $BaTiO_3$, [47,48] and as long as the NW size was larger than a few crystal lattices, smaller NW resulted in stronger piezo-phototronics effect.

A plot on the coupling of geometry size and doping profile was also listed in Fig. 16f. Four lines were plotted, each featuring different NW size and different NW doping. Lower NW doping and smaller NW size both enhanced the piezo-phototronics effect, yet their influence had minor difference. Lower NW doping resulted in a faster enhancement under lower strain, and the current saturated faster. Smaller NW size resulted in a more uniform change over the range of strain values.

Material choices. In optoelectronic devices, heterojunctions were usually utilized to eliminate minority carrier injection and minimize photon reabsorption [49]. As far as band structure was concerned, the major difference between heterojunction and homojunction lay in the discontinuity formed in the interface between different materials and the associated band mismatch. This band discontinuity provides an additional charge potential barrier depending on the materials used. Plus, heterojunctions provided larger reflection in the material interface and was favored in LED fabrications. In the case of piezo-phototronic effect, piezo-charges could help either “recover” or enhance the discontinuity by tuning the local band structure.

n-ZnO NW/p-GaN structure was compared with the n-ZnO/p-ZnO structure to examine the influence of different types of junctions on the optimization of piezo-phototronics effect. From Table 1, the bandgap of ZnO and GaN were similar, leaving similar discontinuity in both valance band and conduction band, which simplified the comparison of simulation result. For a simpler comparison and more intuitive perspective, the result for 1D calculation for heterojunction was shown in Fig. 17a and b for conduction band and valence band as comparison for Fig. 11a. From band structure calculation, the deformation under different strain was similar to the results for a homojunction. In calculation of the device current, the case was much more complicated, as parameters including charge carrier mobility and diffusion constants could be totally different in various materials under various doping condition, and discussion regarding different carrier mobility was too complicated. For simpler comparison, a simulation setting the charge carrier mobility as the same value in GaN was performed and shown in Fig. 17c and d. Fig. 17c showed that the I-V curve under different strain condition was almost identical to that of a homojunction. The curve for current under 6 V bias voltage under different strain conditions were plotted together with that of homojunction in Fig. 17d, which showed the impact of piezo-phototronics effect was slightly stronger in homojunction than in heterojunction, especially when compressive strain was applied, without considering the advantages of heterojunction in optoelectronics or the difference in charge mobility and lifetime between various materials. From simulations displayed in Fig. 12, lower hole mobility on the p-type side was also desired for the piezo-phototronic effect.

Table 1 Material properties used in simulation.

Property	ZnO	GaN
Relative permittivity (ε_r)	9.1	10
Band gap (E_g)/eV	3.38	3.40
Electron affinity (χ)/eV	4.5	4.1
Valence band density of state (N_V)/cm^{-3}	3.5×10^{18}	4.1×10^{19}
Conduction band density of state (N_C)/cm^{-3}	1×10^{20}	1.2×10^{18}
Electron mobility(μ_n)/$m^2V^{-1}s^{-1}$	0.2	0.2
Hole mobility(μ_p)/$m^2V^{-1}s^{-1}$	10^{-3}	10^{-3}

Please cite this article as: Y. Liu, et al., Fundamental theories of piezotronics and piezo-phototronics, Nano Energy (2014), http://dx.doi.org/10.1016/j.nanoen.2014.11.051

ARTICLE IN PRESS

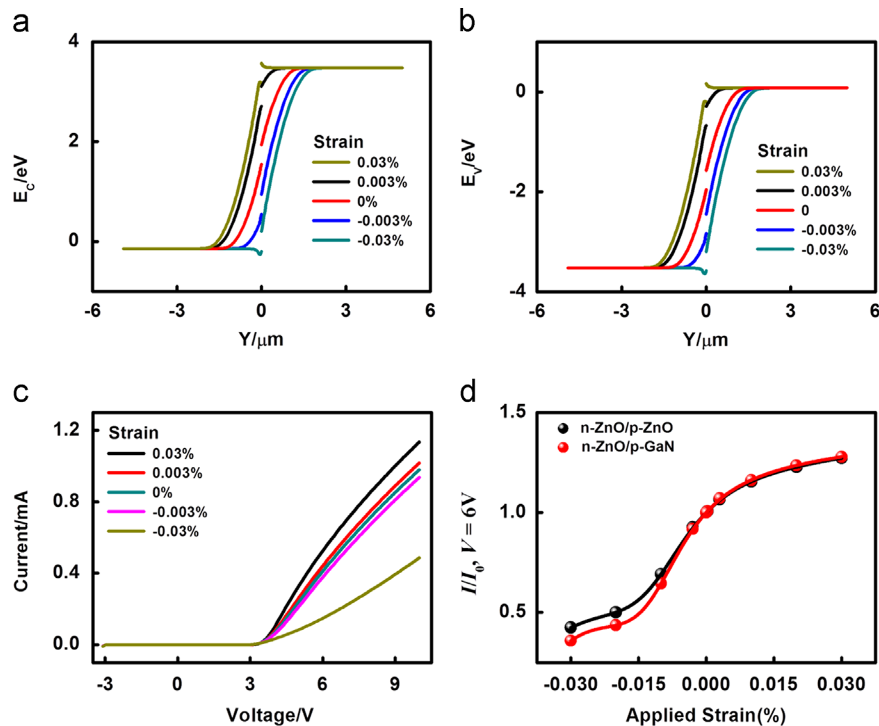

Fig. 17 Simulation results for n-ZnO NW/p-GaN substrate structure, (a) Conduction band deformation of such structure under different strain at n-type side base on 1D simulation, which is chosen for comparison purpose, (b) Valence band deformation of such structure under different strain at n-type side based on 1D simulation, (c) current-voltage characteristics based on 2D simulation, geometry layout and doping are set as the same value as in Fig. 14a, (d) I_{strain}/I_0 vs. ε and comparison with Fig. 14b. Reproduced with permission from Wiley [18].

Summary and perspectives

In summary, the fundamental theoretical principles of piezotronic effect and piezo-phototronic effect have been developed during the past few years. In theoretical analysis, the piezoelectric polarization was discussed in the form of piezo-charges present at an interface of a junction, with three main effects:

a) In metal-semiconductor contact, piezoelectric polarization changes the barrier height and depletion width;
b) In p-n junction, piezoelectric polarization results in shift of depletion region and possibly a change in width;
c) In p-n junction, certain amount of piezoelectric polarization helps form a charge channel near the material interface, which could trap/repel carriers;

Besides piezoelectricity, other factors such as piezoresistance effect and change of contact area or contact condition can also affect the device performance. Through theoretical analysis, the contribution made by the piezoelectric polarization was successfully distinguished from these factors.

Numerical calculations were conducted using the finite element method (FEM), in order to give more intuitive perspective of the piezo-phototronic effect. The band structure and device current-voltage characteristics were successfully simulated. The band structure simulation confirmed the existence of charge channel and depletion shift in piezo-phototronics p-n interface under appropriate straining conditions, which justified the working mechanism of piezotronics/piezo-phototronics effect. The device current simulation not only agreed well with experimental discoveries, but also provided an optimization methodology for material choice and device design.

Based on these basic frameworks, there are a few perspective paths for future theoretical work. For analytical studies, assumptions based on specific kind of material and device can be made to compose models closer to experimental conditions; since the formation of charge channel under strain has been confirmed by simulation, further incorporation of quantum mechanics into the piezotronics and piezo-phototronics theories can help quantify the influence of such charge channel on device performance. It would be really interesting to realize the influence of piezo-charges on single electron transport and spin transport in the quantum regime. For numerical studies, varieties of simulation methods can be utilized for the next step, including finite-difference time-domain (FDTD) methods to calculate optical behaviors in piezo-phototronic devices, as well as first principle calculation to consider quantum effect of piezotronics/piezo-phototronics effect under low temperature measurement and/or 2D materials.

Acknowledgments

Research was supported by BES DOE, NSF, Airforce, Samsung, SKKU (Korea), MANA NIMS (Japan), and the Knowledge Innovation Program of the Chinese Academy of Sciences (KJCX2-YW-M13), the Hightower Chair foundation, and the “thousands talents” program for pioneer researcher and his

Please cite this article as: Y. Liu, et al., Fundamental theories of piezotronics and piezo-phototronics, Nano Energy (2014), http://dx.doi.org/10.1016/j.nanoen.2014.11.051

innovation team, China. The authors thank Prof. Benjamin D.B. Klein in School of Electrical and Computer Engineering in Georgia Tech and Yu Sheng Zhou from School of Materials Science and Engineering in Georgia Tech for their contribution.

References

[1] Z.W. Pan, Z.R. Dai, Z.L. Wang, Science 291 (2001) 1947-1949.
[2] W. Lu, C.M. Lieber, J. Phys. D Appl. Phys. 39 (2006) R387-R406.
[3] C.M. Lieber, Z.L. Wang, Mrs Bull. 32 (2007) 99-108.
[4] Z.L. Wang, Adv. Mater. 19 (2007) 889-892.
[5] Z.L. Wang, Adv. Funct. Mater. 18 (2008) 3553-3567.
[6] Z.L. Wang, Mater. Sci. Eng. R 64 (2009) 33-71.
[7] Z.L. Wang, J. Phys. Chem. Lett. 1 (2010) 1388-1393.
[8] Z.L. Wang, Nano Today 5 (2010) 540-552.
[9] Y.F. Hu, Y. Zhang, Y.L. Chang, R.L. Snyder, Z.L. Wang, Acs Nano 4 (2010) 4220-4224.
[10] Q. Yang, X. Guo, W.H. Wang, Y. Zhang, S. Xu, D.H. Lien, Z.L. Wang, Acs Nano 4 (2010) 6285-6291.
[11] Q. Yang, W.H. Wang, S. Xu, Z.L. Wang, Nano Lett. 11 (2011) 4012-4017.
[12] Q. Yang, Y. Liu, Z.T. Li, Z.Y. Yang, X. Wang, Z.L. Wang, Angew. Chem. Int. Edit. 51 (2012) 6443-6446.
[13] Q. Yang, Y. Liu, C.F. Pan, J. Chen, X.N. Wen, Z.L. Wang, Nano Lett. 13 (2013) 607-613.
[14] F. Zhang, S.M. Niu, W.X. Guo, G. Zhu, Y. Liu, X.L. Zhang, Z.L. Wang, Acs Nano 7 (2013) 4537-4544.
[15] J. Zhou, Y.D. Gu, P. Fei, W.J. Mai, Y.F. Gao, R.S. Yang, G. Bao, Z.L. Wang, Nano Lett. 8 (2008) 3035-3040.
[16] C.F. Pan, L. Dong, G. Zhu, S.M. Niu, R.M. Yu, Q. Yang, Y. Liu, Z.L. Wang, Nat. Photon. 7 (2013) 752-758.
[17] W.Z. Wu, Y.G. Wei, Z.L. Wang, Adv. Mater. 22 (2010) (+)4711 22 (2010) (+).
[18] Y. Liu, S. Niu, Q. Yang, B.D. Klein, Y.S. Zhou, Z.L. Wang (online), Adv. Mater. (2014).
[19] Y. Liu, Q. Yang, Y. Zhang, Z.Y. Yang, Z.L. Wang, Adv. Mater. 24 (2012) 1410-1417.
[20] Y. Zhang, Y. Liu, Z.L. Wang, Adv. Mater. 23 (2011) 3004-3013.
[21] S.M. Sze, Physics of Semiconductor Devices, Wiley, New York, 1981.
[22] T. Ikeda, Fundamentals of Piezoelectricity, Oxford University Press, Oxford, 1996.
[23] G.A. Maugin, Continuum Mechanics of Electromagnetic Solids, North-Holland, Amsterdam, 1988.
[24] R.W. Soutas-Little, Elasticity, XVI, 431, Dover Publications, Mineola, NY, 1999.
[25] COMSOL, "PN Junction 1D", 2014, http://www.comsol.com/model/p-n-junction-benchmark-model-14621.
[26] S. Selberherr, Analysis and Simulation of Semiconductor Devices, Springer, Vienna, 2011.
[27] W. Wu, Y. Wei, Z.L. Wang, Adv. Mater. 22 (2010) 4711-4715.
[28] D.A. Neamen, Semiconductor Physics and Devices: Basic Principles, third ed., McGraw-Hill, Boston, 2003.
[29] E.H. Rhoderick, R.H. Williams, Metal-Semiconductor Contacts, second ed., Clarendon Press; Oxford University Press, Oxford England New York, 1988.
[30] Z.Y. Zhang, K. Yao, Y. Liu, C.H. Jin, X.L. Liang, Q. Chen, L.M. Peng, Adv. Funct. Mater. 17 (2007) 2478-2489.
[31] D.G. Thomas, J.J. Hopfield, Phys. Rev. 116 (1959) 573-582.
[32] X.J. Zhang, W. Ji, S.H. Tang, J. Opt. Soc. Am. B. 14 (1997) 1951-1955.
[33] P.W. Bridgman, Phys. Rev. 42 (1932) 0858-0863.
[34] C.S. Smith, Phys. Rev. 94 (1954) 42-49.
[35] T. Chot, Phys. Status Solidi A. 66 (1981) K43-K45.
[36] C.D. Lien, F.C.T. So, M.A. Nicolet, T. IEEE, Electron. Dev. 31 (1984) 1502-1503.
[37] F. Boxberg, N. Sondergaard, H.Q. Xu, Nano Lett. 10 (2010) 1108-1112.
[38] M.C. Jeong, B.Y. Oh, M.H. Ham, J.M. Myoung, Appl. Phys. Lett. 88 (2006) 202105.
[39] S.N. Mohammad, A.A. Salvador, H. Morkoc, P. IEEE 83 (1995) 1306-1355.
[40] A. Janotti, C.G. Van de Walle, Rep. Prog. Phys. 72 (2009) 126501.
[41] C.I. Wu, A. Kahn, J. Appl. Phys. 86 (1999) 3209-3212.
[42] S.M. Sze, K.K. Ng, Physics of Semiconductor Devices, third ed., Wiley-Interscience, Hoboken, N.J, 2007.
[43] J. Joo, B.Y. Chow, M. Prakash, E.S. Boyden, J.M. Jacobson, Nat. Mater. 10 (2011) 596-601.
[44] C.F. Pan, S.M. Niu, Y. Ding, L. Dong, R.M. Yu, Y. Liu, G. Zhu, Z.L. Wang, Nano Lett. 12 (2012) 3302-3307.
[45] S.M. Niu, Y.F. Hu, X.N. Wen, Y.S. Zhou, F. Zhang, L. Lin, S.H. Wang, Z.L. Wang, Adv. Mater. 25 (2013) 3701-3706.
[46] K. Chakrabarty, S.N. Singh, Solid-State Electron. 39 (1996) 577-581.
[47] W.S. Yun, J.J. Urban, Q. Gu, H. Park, Nano Lett. 2 (2002) 447-450.
[48] J.F. Scott, Science 315 (2007) 954-959.
[49] S.O. Kasap, Optoelectronics and Photonics: Principles and Practices, second ed., Pearson, Boston, 2013.

Dr. Ying Liu received her B.S. degree in Physics from Peking University in 2009 and her Ph.D degree in Materials Science and Engineering from Georgia Institute of Technology in 2014. She is currently a Postdoctoral researcher under supervision of Professor Zhong Lin Wang at Georgia Institute of Technology. Her research interests include theory and experiments of piezotronics and piezo-phototronics, theory of triboelectric generators, hybrid LEDs and hybrid energy harvesting devices.

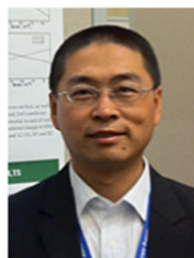

Dr. Yan Zhang received his B.S. degree (1995) and Ph.D degree in Theoretical Physics (2004) from Lanzhou University. Then, he worked as a lecturer, associate Professor (2007), and Professor (2013) of Institute of Theoretical Physics in Lanzhou University. In 2009 he worked as research scientist in the group of Professor Zhong Lin Wang at Georgia Institute of Technology. His main research interests and activities are: self-powered nano/microsystem, theoretical calculation of piezotronic, dynamics of time-delay systems and complex networks.

Dr. Qing Yang received her Bachelor and Ph.D. degree in Materials Science and Engineering from Zhejiang University in 2006. She worked as a visiting scientists in Material Science and Engineering at Georgia Institute of Technology from 2009 to 2012. Currently, she is a Professor in the. Her research focuses on micro-/nano-photonics, piezo-phototronics and flexible nanosystems.

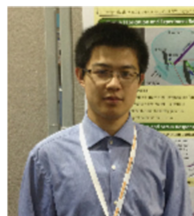

Simiao Niu is a Ph.D. candidate working as a graduate research assistant in School of Materials Science and Engineering at the Georgia Institute of Technology, under the supervision of Dr. Zhong Lin Wang. He earned his bachelor of engineering degree in the Institute of Microelectronics at Tsinghua University in

ARTICLE IN PRESS

2011 with the highest honors and outstanding undergraduate thesis award. His doctoral research interests include theoretical and experimental studies on: mechanical energy harvesting by triboelectric nanogenerators and high-performance piezotronic and piezo-phototronic sensors based on piezoelectric nanowires.

Dr. Zhong Lin (ZL) Wang is the Hightower Chair in Materials Science and Engineering, Regents' Professor, at Georgia Tech. He is also the chief scientist and director of Beijing Institute of Nanoenergy and Nanosystems, Chinese Academy of Sciences. Dr. Wang has made original and innovative contributions to the synthesis, discovery, characterization and understanding of fundamental physical properties of oxide nanobelts and nanowires, as well as applications of nanowires in energy sciences, electronics, optoelectronics and biological science. He is the leader figure in ZnO nanostructure research. His discovery and breakthroughs in developing nanogenerators establish the principle and technological road map for harvesting mechanical energy from environment and biological systems for powering a personal electronics. His research on self-powered nanosystems has inspired the worldwide effort in academia and industry for studying energy for micro-nano-systems, which is now a distinct disciplinary in energy research and future sensor networks. He coined and pioneered the field of piezotronics and piezo-phototronics by introducing piezoelectric potential gated charge transport process in fabricating new electronic and optoelectronic devices. This historical breakthrough by redesign CMOS transistor has important applications in smart MEMS/NEMS, nanorobotics, human-electronics interface and sensors. Wang also invented and pioneered the in-situ technique for measuring the mechanical and electrical properties of a single nanotube/nanowire inside a transmission electron microscope (TEM).

Please cite this article as: Y. Liu, et al., Fundamental theories of piezotronics and piezo-phototronics, Nano Energy (2014), http://dx.doi.org/10.1016/j.nanoen.2014.11.051